

Constraints on gas giant satellite formation from the interior states of partially differentiated satellites

Amy C. Barr*, Robin M. Canup

Department of Space Studies, Southwest Research Institute, 1050 Walnut St., Suite 300, Boulder, CO 80302, USA

ARTICLE INFO

Article history:

Received 2 October 2007

Revised 20 June 2008

Available online 3 August 2008

Keywords:

Callisto

Jupiter

Saturn

ABSTRACT

An icy satellite whose interior is composed of a homogeneous ice/rock mixture must avoid melting during its entire history, including during its formation when it was heated by deposition of accretional energy and short-lived radioisotopes. Estimates of the temperature rise associated with radiogenic and accretional heating, coupled with limits on satellite melting can be used to constrain the timing of formation of a partially differentiated satellite relative to the origin of the calcium–aluminum-rich inclusions (CAI's) as a function of its accretion timescale and the protosatellite disk temperature (T_d). Geological characterization and spacecraft radio tracking data suggest that Callisto, the outermost regular satellite of Jupiter, and Saturn's mid-sized satellite Rhea, are partially differentiated if their interiors are in hydrostatic equilibrium. Because the specific conditions during the satellites' formation are uncertain, we determine accretional temperature profiles for a range of values for T_d and accretion time scales with the limiting assumption that impactors deposit all their energy close to the surface, leading to maximally effective radiative cooling. We find that Callisto can remain unmelted during formation if it accreted on a time scale longer than 0.6 Myr. Considering both radiogenic and accretional heating, Callisto must have finished accreting *no earlier* than ~ 4 Myr after formation of CAI's for $T_d = 100$ K. Warmer disks or larger impactors that deposit their energy at depth in the satellite would require longer and/or later formation times. If Rhea accreted slowly (in 10^5 to 10^6 years), its growth must have finished no earlier than ~ 2 Myr after CAI's for $70 \text{ K} \leq T_d \leq 250 \text{ K}$ to avoid early melting. If Rhea formed quickly ($\leq 10^3$ yr), its formation must have been delayed until at least 2 to 7 Myr after CAI's and in a disk with $T_d < 190$ K in the small impactor limit. If the satellites form in slow-inflow-supplied disks as proposed by Canup and Ward [Canup, R.M., Ward, W.R., 2002. *Astron. J.* 124, 3404–3423], the implied satellite ages suggest that gas inflow to the giant planets ceased no earlier than ~ 4 Myr after CAI's, comparable to average nebular lifetimes inferred from observations of circumstellar disks.

© 2008 Elsevier Inc. All rights reserved.

1. Introduction

Satellites whose interiors contain a homogeneous mixture of ice and rock provide a unique opportunity to constrain the timing and duration of their formation. A partially differentiated icy satellite must have avoided ice melting during its entire history, including during formation when its surface is heated by accretional impacts; the amount of heating depends on the accretion time scale, impactor size, and impactor velocity. Growing satellites also receive a burst of energy in their interiors from the decay of short-lived radioisotopes such as ^{26}Al . A large satellite that is currently partially differentiated must have formed slowly, so that its accretional energy can be radiated away between successive impacts, and relatively late in Solar System history to avoid internal melting from heating by short-lived radioisotopes. If the satellites

form in the final stages of giant planet gas accretion at the end of the lifetime of the solar nebula (e.g., Canup and Ward, 2002, 2006), constraints on the endpoint of satellite accretion can constrain the timing of giant planet formation relative to the formation of calcium–aluminum-rich inclusions (CAI's), inferred to be the oldest solid materials in the Solar System.

All four Galilean satellites have roughly similar masses and have an increasing mass fraction of ice with increasing radial distance from Jupiter. Innermost Io, Europa, and Ganymede are in a mutual Laplace resonance, and have been physically and chemically processed by tidal dissipation, which has also driven global endogenic resurfacing (McEwen et al., 2004; Greeley et al., 2004; Pappalardo et al., 2004). Icy Ganymede is fully differentiated, with a metallic core and rocky mantle, overlain by rock-free ice (Schubert et al., 2004). Outermost Callisto (semi-major axis $a = 26R_J$ where R_J is Jupiter's radius, and satellite radius $R_s = 2410$ km) shows no evidence of endogenic resurfacing (Moore et al., 2004), and early work interpreted Callisto's ancient surface as evidence for an

* Corresponding author. Fax: +1 (303) 546 9687.

E-mail address: amy@boulder.swri.edu (A.C. Barr).

undifferentiated interior (Schubert et al., 1981). Subsequent work suggests that tides may be a key driving force for endogenic resurfacing on icy satellites, so Callisto's surface cannot be interpreted as definitive evidence for a primitive interior (see Pappalardo et al., 2004 for discussion). However, close flybys of Callisto during the *Galileo* mission provided further evidence for an undifferentiated interior, giving an estimate of its moment of inertia constant $C/MR^2 = 0.3549 \pm 0.0042$ (Anderson et al., 2001) assuming hydrostatic equilibrium, which is midway between the value for fully differentiated Ganymede, $C/MR^2 = 0.3115 \pm 0.0028$ (Schubert et al., 2004), and a value appropriate for a homogeneous-density Callisto accounting for compression of ice at depth, $C/MR^2 = 0.38$ (McKinnon, 1997). In the simplest interpretation of Callisto's C/MR^2 value, its interior consists of a homogeneous ice/rock mixture beneath an outer shell of rock-free ice ~ 300 km thick (Anderson et al., 2001; Schubert et al., 2004).

Voyager images of saturnian satellite Rhea ($a = 8.7R_{\text{Saturn}}$, $R_s = 765$ km) suggest that it has an old and heavily cratered surface that records only limited evidence of endogenic resurfacing (Moore et al., 1985). A relatively inactive Rhea is supported by crater counting using *Cassini* images, which suggests an old surface (Kirchoff and Schenk, 2008), and Rhea's limited interaction with Saturn's magnetic field (Khurana et al., 2008). *Cassini* data suggest that Rhea is partially differentiated and much of its interior consists of a homogeneous mixture of ice and rock (Anderson and Schubert, 2007; less et al., 2007), although this interpretation assumes hydrostatic equilibrium which may not be valid for Rhea (Mackenzie et al., 2008).

A rough estimate of the energy liberated within a satellite during formation is given by the gravitational binding energy per unit mass, $E_a \sim 3/5(GM_s/R_s)$, where M_s is the satellite's mass and G is the gravitational constant. Callisto's binding energy $E_a \sim 2 \times 10^6 \text{ J kg}^{-1}$ is roughly $6 \times$ the latent heat of fusion of water ice ($\sim 3 \times 10^5 \text{ J kg}^{-1}$), suggesting that its icy component should melt during formation if all of its accretional energy is retained. Rhea, which is a much smaller satellite, can avoid melting due to accretional energy because $E_a \sim 10^5 \text{ J kg}^{-1}$, sufficient to raise the temperature of its icy component ($C_p = 2100 \text{ J kg}^{-1}$) by only 60 K. Although accretional energy alone may not be sufficient to melt Rhea, accretional and radiogenic heating combined may be able to drive global melting in Rhea's interior early in its history.

Existing models of the thermal evolution of growing satellites rely on a simple approach wherein a poorly constrained fraction “ h ” of energy deposited by accretional impacts is retained and used to heat the satellite (Kaula, 1979; Stevenson et al., 1986). This and similar approaches have been used to estimate accretional heating in both Rhea and Callisto (Schubert et al., 1986; Stevenson et al., 1986; Squyres et al., 1988). For $h \sim 0.1$, corresponding to small impactors that deposit their energy close to the satellite's surface, it is possible to obtain unmelted callistos (e.g., Stevenson et al., 1986). However, it has not been known whether such a low value of h is realistic. If Callisto avoids accreting a substantial gaseous envelope, its surface can cool by radiation, and if it also forms slowly (accretion time scale $\tau_{\text{acc}} \geq 10^5$ yr) and/or from small satellitoids, it may be possible for it to avoid melting during formation (Stevenson et al., 1986). Aluminum-26 alone provides enough heat to melt the ice in Callisto unless it formed after the decay of ^{26}Al , some 2.6 to 3 Myr after CAI condensation (McKinnon, 2006b). Although prior studies have placed loose constraints on the timing and duration of Callisto's accretion, none have included both accretional energy and ^{26}Al heating.

Squyres et al. (1988) applied a modified “ h ” parameterization to determine accretional temperature profiles for rheas that form in < 1000 yr in a minimum-mass subnebula (described in Section 2.1) around Saturn. Squyres et al. (1988) assumed that ~ 20 to 60% of the impact energy was retained at depth to heat the satellite,

and the remainder deposited at the surface where it was subject to radiative cooling. In such a model, Rhea reaches a maximum temperature of 215 to 225 K at a depth of 25 to 90 km below its surface. Although these results suggest that Rhea avoids melting during formation, several assumptions in Squyres' work may have led to unrealistically cold rheas. Squyres et al. (1988) assumed that the temperature of material accreting onto Rhea was essentially negligible compared to the satellite's temperature and also ignored radiogenic heating. However, nebular temperatures could have yielded accreting material that was substantially warmer. Recent satellite evolution models linking the current state of Iapetus to early heating from short-lived radioisotopes (Castillo-Rogez et al., 2007) require formation times for the saturnian system as early as 2.5 Myr after CAI formation. As we will show below, Rhea experiences melting during formation if its accretion is rapid, occurs in a warm disk, and occurs early in Solar System history. For example, if Rhea formed in a disk with a mid-plane disk temperature $T_d \gtrsim 100$ K (see Fig. 1), from impactors having comparable interior temperatures, finished forming 2.5 Myr after CAI's, and retained all of its ^{26}Al and accretional heating, its temperature would be raised to $\gtrsim 260$ K.

Considering both accretional and radiogenic heating, we show that callistos and rheas formed from small impactors, over long time scales, and in cold disks can remain unmelted during formation for reasonable start times relative to CAI condensation, accretion time scales, and protosatellite disk temperatures. For Rhea, fast accretion can also be consistent with limited melting, although in this case, more restrictive constraints on T_d and/or accretion start times apply than for the slow accretion case. We find that Rhea and Callisto can remain unmelted even if ammonia is present in their interiors. Finally, we show that conditions consistent with an undifferentiated Callisto can create melted ganymedes, suggesting that the differences between their interior states could be primordial.

2. Formation environment

The ranges of accretion time scales and protosatellite disk temperatures we consider are motivated by several different scenarios for conditions in the gas giant protosatellite disk: the traditional minimum-mass subnebula model (e.g., Lunine and Stevenson, 1982; Pollack and Consolmagno, 1984), the solid-enhanced minimum mass (SEMM) model (Mosqueira and Estrada, 2003), and the slow inflow/gas-starved disk model (Canup and Ward, 2002, 2006). The rate of mass accretion (\dot{M}) onto a growing satellite of radius r is $\dot{M} \approx \sigma_S \Omega \pi r^2 F_g$, where σ_S is the surface mass density of solid ices and rock in the disk, Ω is the satellite's orbital frequency ($\Omega = \sqrt{GM_p/a^3}$, with M_p the planet's mass and a the satellite's semi-major axis), and $F_g = 1 + (v_{\text{esc}}/v_\infty)^2 \geq 1$ is the gravitational focusing factor, which is a function of the characteristic relative velocity of accreting material, v_∞ , and the escape velocity of the satellite, v_{esc} . The satellite formation time scale $\tau_{\text{acc}} = M/\dot{M} = 4/3(1/F_g)(\bar{\rho}r/\sigma_S)\Omega^{-1}$.

2.1. Minimum-mass subnebula

Historically, satellite formation models focus on the evolution of a minimum-mass subnebula (MMSN), wherein the masses of the currently observed satellites are combined with gas to create a massive solar-composition disk around the parent planet (e.g., Lunine and Stevenson, 1982; Coradini et al., 1989). A MMSN disk at Rhea's location has $\sigma_S \sim 10^3$ to 10^4 kg m^{-2} (e.g., Squyres et al., 1988), implying $\tau_{\text{acc}} \sim 500 \text{ yr} (1/F_g)(\bar{\rho}/1233 \text{ kg m}^{-3})(r/765 \text{ km}) \times (5 \times 10^3 \text{ kg m}^{-2}/\sigma_S)$. A jovian MMSN has $\sigma_S \sim 10^4$ to 10^5 kg m^{-2} at Callisto's location (e.g., Coradini et al., 1989; Canup and Ward,

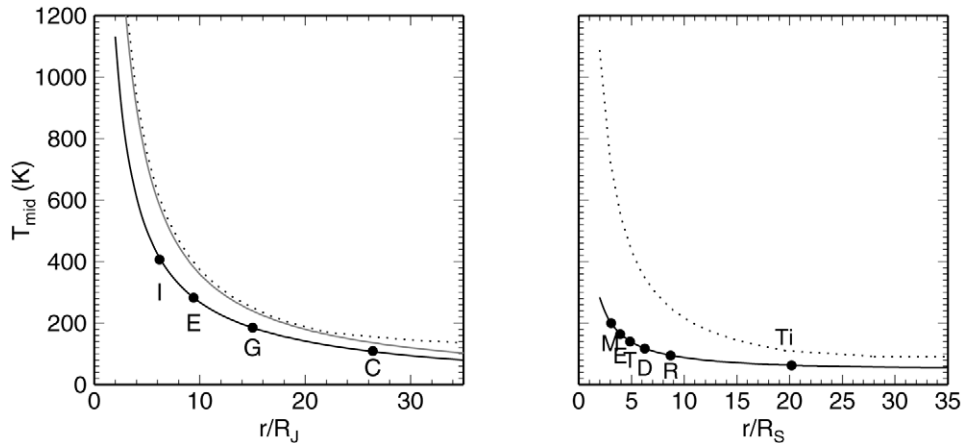


Fig. 1. (Left) Sample midplane temperatures for the CW model (solid line, after Canup and Ward, 2008) for the time period of Galilean satellite accretion, assuming a gas-to-solids ratio in the inflow $f \sim 100$, an exponentially decaying inflow with $\tau_{\text{in}} = 10^6$ yr, a disk viscosity alpha parameter $\alpha = 0.006$, an ambient temperature $T_{\text{neb}} = 20$ K, planetary temperature $T_p = 500$ K (e.g., Burrows et al., 1997), and a solar composition dust opacity (i.e., Planck and Rosseland opacities $\kappa_B \sim \kappa_R \sim 1$). See Appendix A for details. Dotted line shows the temperature profile for the subjovian nebula model from Fig. 3 of Mosqueira and Estrada (2003). Letters indicate present positions of Io, Europa, Ganymede, and Callisto. (Right) Midplane temperatures in the inner circumjovian disk in the CW model (solid line) during the formation of the inner saturnian satellites with $\tau_{\text{in}} = 10^6$ Myr, $\alpha = 0.006$, $T_p = 400$ K, $T_{\text{neb}} = 20$ K, and $\kappa_B \sim \kappa_R \sim 1$. Dotted line shows the saturnian disk temperature profile from Fig. 3 of Mosqueira and Estrada (2003). Letters indicate the present locations of Mimas, Enceladus, Tethys (T), Dione, Rhea, and Titan (Ti).

2002), implying an accretion time scale $\tau_{\text{acc}} \sim 800$ yr $(1/F_g) \times (\bar{\rho}/1800 \text{ kg m}^{-3})(r/2410 \text{ km})(5 \times 10^4 \text{ kg m}^{-2}/\sigma_S)$. Such short accretion time scales result in ice melting, if not complete ice vaporization, during the formation of Ganymede- and Callisto-sized satellites (Stevenson et al., 1986). It is seemingly impossible to create an undifferentiated ice-rock callisto in a traditional MMSN. Traditional MMSN models for the Galilean satellites also face a number of other challenges (see Canup and Ward, 2002 for discussion).

MMSN models predict dense, gas-rich protosatellite disks and typically assume a radial disk temperature profile $T_d \propto r^{-1}$ (see e.g., Fig. 1), with suggested values at Rhea’s distance ranging from $T_d \sim T_{\text{neb}}$ where T_{neb} is the solar nebula temperature at Saturn’s orbit during satellite accretion, to $T_d \sim 250$ K (Pollack and Consolmagno, 1984). In a jovian MMSN disk, $T_d \sim 150$ K is a commonly quoted value at Callisto’s location (Lunine and Stevenson, 1982; Mosqueira and Estrada, 2003). The sizes of the impactors that assemble satellites in a MMSN are not well-understood, but could be large.

Disk temperatures quoted for the SEMM, which are based on a heuristic disk model, are similar to those quoted for the MMSN (see Fig. 1). In the Mosqueira and Estrada (2003) model, Callisto forms in the outer disk on a timescale controlled by the time it takes gas drag to clear the outer disk of embryos, giving $\tau_{\text{acc}} \sim 10^6$ yr. They estimate that Ganymede forms more quickly within the inner disk, in 10^3 to 10^4 years, while for Titan, $\tau_{\text{acc}} \sim 10^4$ to 10^5 yr. For Callisto, Mosqueira and Estrada (2003) estimate characteristic impactor sizes of 300 to 500 km, although the actual size may be smaller because this calculation does not include fragmentation (I. Mosqueira, personal communication).

2.2. Gas-starved disk

An alternative approach (Canup and Ward, 2002, 2006) considers satellite growth in a “gas-starved” disk supplied by the slow inflow of gas and ≤ 1 meter-sized rock and ice particles from solar orbit. Recent models of gas giant planet formation suggest that Jupiter and Saturn contracted to a scale similar to their current sizes before the solar nebula dissipated (e.g., Papaloizou and Nelson, 2005). In this case, during the final stages of a gas giant’s growth, gas and small entrained particles in solar orbit flow

into the growing planet’s Hill sphere and produce a circumplanetary disk (e.g., Lubow et al., 1999). In the Canup and Ward model (hereafter CW), once the gas and small particles achieve planetary orbit, the gaseous component is assumed to spread viscously, both inward onto the growing gas giant, and outward. As the disk is continuously supplied with new material from solar orbit, the gas density in the disk achieves a quasi-steady state. Solids become concentrated in the disk over time because ice/rock particles quickly grow to sizes large enough to become decoupled from the gas, and so remain in orbit around the planet where they are swept up by accreting satellites.

Direct accretion simulations demonstrate that such conditions produce Galilean- and saturnian-like satellite systems, and show that during inflow, multiple generations of satellites can be created with all but the last colliding with the growing planet (Canup and Ward, 2006). Assuming that the inflow decays with time, the final Galilean and saturnian satellites then form during the waning stages of Jupiter and Saturn’s gas accretion (Canup and Ward, 2002, 2006). This implies that the observed satellites formed in a disk with a much lower gas density than suggested by MMSN models, and that the satellites accreted slowly, at a rate controlled by the final inflow rate of solids to the disk.

Suppose that gas and solid inflow to the disk decays exponentially with time constant τ_{in} , so that the mass inflow rate $F_*(t) = F_*(0) \exp(-t/\tau_{\text{in}})$. The total mass delivered to the disk after time t' is $M_{\text{in}}(t') = \int_0^{t'} F_*(t) dt = F_*(t') \tau_{\text{in}}$. The final generation of satellites, which contains a mass M_T in solids, forms at a time t_s when the inflow rate has decayed so that $M_{\text{in}}(t_s) = f M_T$, where f is the gas-to-solids ratio in the inflow, implying $F_*(t_s) = f(M_T/\tau_{\text{in}})$. For an exponentially decaying inflow, the satellite accretion timescale is $\tau_{\text{acc}} \sim \tau_{\text{in}}$. If τ_{in} is set by the dispersal of the solar nebula, $\tau_{\text{acc}} \sim \tau_{\text{in}} \sim 10^6$ to 10^7 yr (Haisch et al., 2001). Alternatively, a maximum inflow rate can be derived from the icy satellites’ compositions because disk temperatures depend on the mass inflow rate (Canup and Ward, 2002, 2008; see also Appendix A).

Prior works consider the lower limit on the temperatures in the protosatellite disks at Jupiter and Saturn to be the solar nebula temperatures at the parent planets’ locations, $T_{\text{neb}} \sim 100$ to 150 K for Jupiter, and $T_{\text{neb}} \sim 90$ K at Saturn (Lewis, 1974; Garaud and Lin, 2007). However, if Jupiter and Saturn opened gaps in the solar nebula (e.g., Bate et al., 2003), their disks could radiate predominantly into a colder, ~ 20 K background (D’Angelo et

al., 2003). During inflow, the disk is heated by the planet's luminosity, viscous dissipation, and the release of potential energy of infalling material. Fig. 1 shows example temperature profiles for protosatellite disks at Jupiter and Saturn in the CW model created by solar-composition inflows ($f \sim 100$) with $\tau_{\text{in}} = 10^6$ yr. Details of the thermal model used to generate the CW curves are given in Appendix A. The jovian disk in Fig. 1 is shown at time t_s after which the last mass in solids equal to that of the Galilean satellites ($M_T = 2 \times 10^{-4} M_J$) will be delivered by an exponentially decaying inflow (i.e., $M_{\text{in}}(t_s) = 2 \times 10^{-4} f M_J$). The inner saturnian satellites (Mimas, Enceladus, Tethys, Dione, and Rhea) have a total mass $M_T \sim 7 \times 10^{-6} M_S$. Their formation is predicted to occur after the formation of Titan in the CW model (see Appendix A). Fig. 1 shows the saturnian disk at the time after which a final mass of $f(7 \times 10^{-6}) M_S$ is delivered to the disk interior to $15 R_{\text{Saturn}}$, assuming a uniform inflow per area across the disk and an outer radius of the inflow region $\sim 30 R_{\text{Saturn}}$ (e.g., Canup and Ward, 2002, 2006).

Slow accretion in a cold gas-starved disk does not guarantee the creation of unmelted satellites. Callisto must be assembled from objects small enough to deposit most of their heat near the surface where it can be removed by radiative cooling. Small impactors also promote the creation of a homogeneous ice/rock interior: for example, if Callisto is assembled from fully differentiated satellitesimals, the large fragments of rock in the centers of the impactors may sink through the ice/rock mantle, causing slow differentiation (see Nagel et al., 2004 for discussion). In Appendix B, we estimate the characteristic impactor size r_{par} in the CW model by assuming a balance between the rate of particle supply to the disk, rate of particle collision with the growing satellite, and rate of collision between particles within the disk. We find characteristic impactor sizes at Rhea of 1 m, comparable to the largest particles that would flow into the saturnian nebula with the gas (Canup and Ward, 2002). Impactors that assemble Callisto are estimated to have radii of $\sim 0(1)$ km or less, depending on the fraction of particle-particle collisions that result in accretion vs fragmentation.

2.3. Range of accretion conditions

Given the variety of suggested formation scenarios for the Galilean and saturnian satellites, we model the thermal evolution of satellites growing in a wide range of conditions. We consider temperatures at Rhea's location ranging from $T_d = 70$ K to $T_d = 250$ K and at Callisto's location ranging from $T_d = 70$ K to $T_d = 165$ K. We also explore accretion time scales between 10^3 yr appropriate for MMSN disks, and $\tau_{\text{acc}} \sim$ the approximate upper limit on the lifetime of the solar nebula of 10^7 yr (Haisch et al., 2001), the longest time appropriate for inflow-regulated accretion.

3. Constraints

The simplest interpretation of Callisto's moment of inertia constant suggests that its inner ~ 2000 km consists of a mixture of rock and ice. However, the interpretation of Callisto's moment of inertia is uncertain. Because all of the *Galileo* Callisto flybys were nearly equatorial and because Callisto is a slow rotator (Schubert et al., 2004), it was not possible to obtain independent estimates of J_2 and C_{22} to determine whether Callisto is in hydrostatic equilibrium. The moment of inertia coefficient reported by Anderson et al. (2001) was obtained from radio tracking data under the assumption of hydrostatic equilibrium. This assumption may be reasonable given Callisto's size (Anderson et al., 2001; Schubert et al., 2004), but it should be noted that a non-hydrostatic figure (for example, the presence of mass anomalies at the surface of a rocky core) could potentially mask a higher degree of differentiation (Mueller and McKinnon, 1988; McKinnon, 1997).

If the ice component of Callisto's interior melts, rock particles will rapidly sink to the bottom of the melted region, resulting in local differentiation. Due to uncertainties in differentiation dynamics in icy bodies, it is not clear whether successive local differentiation events could trigger global ice-rock separation, but this is certainly a possibility for Callisto (Lunine and Stevenson, 1982; Mueller and McKinnon, 1988). The energy of differentiating Callisto is $\sim 2.5 \times 10^5 \text{ J kg}^{-1}$, sufficient to raise its interior temperature by ~ 170 K, so that even partial differentiation could contribute significantly to its heat budget (Friedson and Stevenson, 1983). If the temperature of Callisto's interior is warmed close to the ice melting point, slow differentiation can occur due to downward sinking of co-accreted rock particles by Stokes flow. The Stokes flow velocity is proportional to the square of the radius of the rock particle, so the rocks in Callisto's interior must be relatively small to avoid settling out over the accretional time scale. The Stokes flow velocity is also inversely proportional to the ice viscosity, which is strongly temperature-dependent (Durham et al., 1997). If the high-pressure ice polymorphs in Callisto's interior were warmed close to their melting points, the ice mantle viscosity is plausibly $\eta \sim 10^{16}$ to 10^{17} Pa s, allowing a boulder of radius b to sink at a velocity of $\sim 30 \text{ m yr}^{-1} (b/5 \text{ km})^2 (10^{16} \text{ Pa s}/\eta)$. A 5 km-radius boulder can traverse the satellite radius in only $\sim 10^5$ yr. This argues for satellite assembly from homogeneous ice/rock bodies rather than from fully differentiated parent bodies with large rock cores. In the CW model, we expect that Callisto's impactors will themselves be undifferentiated because their gravitational binding energies are extremely small, $E_a \sim 3/5(GM_{\text{par}}/r_{\text{par}}) \sim 1 \text{ J kg}^{-1}$ for $r_{\text{par}} \sim 1$ km.

Accreting Callisto from small ice/rock impactors and keeping its interior as cold as possible to keep its ice highly viscous during its early evolution seems to be the most straightforward way to avoid slow ice-rock separation during accretion. Based on its moment of inertia factor and the energetics of its differentiation, we consider it likely that Callisto must avoid melting altogether in order to avoid runaway differentiation and impose the constraint that Callisto's temperature must remain below the melting point as it forms. We do not shed light on whether Callisto's present ocean (Zimmer et al., 2000) formed during accretion, or later in its history as its interior was warmed by long-lived radiogenic heating.

A number of conflicting interpretations for the gravity data obtained during the November, 2005 flyby of Rhea have been proposed. Anderson and Schubert (2007) derive a moment of inertia for Rhea of $C/MR^2 = 0.3911 \pm 0.0045$ by reducing the radio tracking data under the assumption of hydrostatic equilibrium. Iess et al. (2007) perform similar analyses and find $C/MR^2 = 0.3721 \pm 0.0036$. A recent re-evaluation of the radio tracking and navigation data without an *a priori* assumption of hydrostatic equilibrium suggests $J_2/C_{22} \sim 3.7$ to 3.9, larger than the 10/3 value consistent with hydrostatic equilibrium (Mackenzie et al., 2008). Nimmo and Matsuyama (2007) suggest that reorientation of Rhea due to torques from uncompensated impact basins may lead to substantial contributions to its gravity signature and complicate the interpretation of the radio tracking data. At present, a non-hydrostatic Rhea is not a foregone conclusion; a rebuttal paper addressing the methods of Mackenzie et al. (2008) is currently in preparation (G. Schubert, personal communication). Assuming hydrostatic equilibrium, both moment of inertia values suggest model rheas that are incompletely differentiated. If the interior of Rhea consists of a homogeneous ice/rock core and near-surface rock-free layer, the thickness of its outer pure ice layer, z_{ice} , would be $z_{\text{ice}} = 46 \pm 24$ km thick (adopting $C/MR^2 = 0.3911$, ice density $\rho_i = 1000 \text{ kg m}^{-3}$, and rock density $\rho_r = 3000 \text{ kg m}^{-3}$), or $z_{\text{ice}} = 158 \pm 23$ km thick (adopting $C/MR^2 = 0.3721$). For Rhea, we apply the constraint that melting can occur only in its outer 46 or 158 km.

Table 1
Satellite parameters

Parameter	Symbol	Ganymede	Callisto	Rhea
Parent planet mass	M_p	1.90×10^{27} kg	1.90×10^{27} kg	5.68×10^{26} kg
Parent planet radius	R_p	71,938 km	71,938 km	60,330 km
Satellite orbital distance	a/R_p	15	26.4	8.7
Orbital frequency	Ω	1.01×10^{-5} s ⁻¹	4.36×10^{-6} s ⁻¹	1.61×10^{-5} s ⁻¹
Satellite radius	R_s	2631 km	2410 km	765 km
Satellite mass	M_s	1.48×10^{23} kg	1.07×10^{23} kg	2.30×10^{21} kg
Mean density	$\bar{\rho}$	1942 kg m ⁻³	1834 kg m ⁻³	1233 kg m ⁻³

Table 2
Assumed properties of satellite interiors

Parameter	Symbol	Ganymede	Callisto	Rhea
Rock density	ρ_r	3000 kg m ⁻³	3000 kg m ⁻³	3000 kg m ⁻³
Ice density	ρ_i	1400 kg m ⁻³	1400 kg m ⁻³	1000 kg m ⁻³
Rock mass fraction	m_r	0.52	0.44	0.28
Specific heat	C_p	1370 J kg ⁻¹ K ⁻¹	1480 J kg ⁻¹ K ⁻¹	1700 J kg ⁻¹ K ⁻¹

4. Methods

4.1. Accretional temperature profiles

To determine accretional temperature profiles within a growing satellite, we balance radiation from its surface, heating of impacted material from its initial temperature (which we assume = T_d) to the satellite's time-dependent surface temperature T , and accretional heating (Squyres et al., 1988),

$$\bar{\rho} C_p (T - T_d) \frac{dr}{dt} = \frac{1}{2} \frac{\dot{M} u_i^2}{4\pi r^2} - \sigma_{\text{SB}} (T^4 - T_d^4), \quad (1)$$

where r is the time-dependent satellite radius, σ_{SB} is the Stefan-Boltzmann constant, C_p is the specific heat, T_d is the ambient temperature in the protosatellite disk, $\bar{\rho}$ is the satellite mean density, and u_i is the impact velocity. Equation (1) assumes that the growing satellite radiates into an optically thick disk (see Appendix A). The impact velocity is $u_i^2 = v_{\text{esc}}^2 + v_{\infty}^2$, where we assume v_{∞} is a function of the time-dependent satellite escape velocity, $v_{\text{esc}}^2 = 2GM(t)/r(t)$, as $v_{\infty} = v_{\text{esc}}/2$, which corresponds to a gravitational focusing factor $F_g = 1 + (v_{\text{esc}}/v_{\infty})^2 = 5$ (see Appendix B). For each satellite we also include radiogenic heating, discussed below. Values of the physical properties of the satellites are summarized in Tables 1 and 2. The spherical symmetry of Eq. (1) implies that the energy deposited from a single impact is averaged over the satellite's surface, a good assumption if accretion is due to a large number of uniformly distributed impactors.

Squyres et al. (1988) define an η parameter analogous to the “ h ” used in earlier works (Schubert et al., 1986; Stevenson et al., 1986) as the fraction of impact energy deposited at depth within the satellite where it is not subject to radiative cooling. In the limit of small impactors that deposit energy very close to the satellite's surface, $\eta \sim 0$, which is the implicit assumption in Eq. (1) above. Here, we solve Eq. (1) in the limit $\eta \rightarrow 0$ to determine the *minimum* $T(r)$ for a given set of formation conditions, which will allow us to estimate the earliest start time for satellite accretion, the shortest possible accretion time scale, and the warmest disk consistent with Callisto and Rhea's interior states. If Callisto or Rhea were assembled from large bodies, the effective η would increase, and more impact heat would be retained within the satellite (see discussion in Squyres et al., 1988), leading to more restrictive constraints on the timing and/or duration of the satellites' formation.

Equation (1) does not include solid-state heat transport by diffusion or solid-state convection. Diffusion will transport heat over a characteristic length scale of only $\sim \sqrt{\kappa \tau_{\text{acc}}} \leq 30$ km for $\tau_{\text{acc}} \leq 10^7$ yr (using a thermal diffusivity for warm ice $\kappa = 2.6 \times 10^{-6}$ m² s⁻¹). A growing satellite is heated mostly from its surface

by accretional energy. This leads to a temperature gradient in the opposite sense than that required for convection—a surface-heated ice or ice/rock mantle of uniform rock content with depth is gravitationally stable and will not convect. Radiogenic heating in the satellite's interior may drive convection in its core, but it is unlikely that convection can start on a time scale shorter than the satellite accretion time. The onset time for convection in the satellites' interiors (t_o) can be estimated as a function of its physical and rheological parameters (Zaraneek and Parmentier, 2004),

$$t_o \approx \frac{500}{\kappa} \left(\frac{\bar{\rho} \alpha \Delta T_i g}{\eta_o \kappa} \right)^{-2/3}, \quad (2)$$

where $\Delta T_i \sim 20$ K is the approximate magnitude of the temperature variations available to drive convection in the satellite's core, g is the local gravitational acceleration, α is the coefficient of expansion of water ice, and η_o is the ice viscosity. Ice I is the dominant ice phase in Rhea's core, where the central pressure is 124 MPa. The lower limit on the onset time for convection in Rhea's interior $t_o \sim 3 \times 10^6$ yr is obtained using the surface gravity $g = 0.26$ m s⁻², and $\eta_o = 10^{14}$ Pa s, the melting point viscosity of ice I deforming due to diffusion creep with a grain size of 1 mm (Goldsby and Kohlstedt, 2001). At the center of a homogeneous Callisto, ice VII is the dominant phase, but very little is known about its rheology. If we suppose that the rheology of ice VII is similar to ice V and VI, its melting point viscosity $\eta_o \sim 10^{17}$ Pa s (Durham et al., 1997). Assuming that the thermodynamic properties of the high-pressure polymorphs are similar to ice I, $\alpha \approx 10^{-4}$ K⁻¹, $\kappa \approx 10^{-6}$ m² s⁻¹ (Kirk and Stevenson, 1987). In the innermost core, $g \sim 0.1$ m s⁻², which gives $t_o \sim 10^8$ yr. Because the onset time of convection is much longer than likely accretional time scales, we do not expect convection to substantially affect accretional temperature profiles in either satellite. We do not include latent heat in the satellite's energy budget because we seek to determine the value of r at which the satellite melts during its formation; once melting occurs, the simulation is ended.

The amount of radiogenic heating in the satellite's interior depends on the time at which a layer at radius r forms,

$$t_f(r) = t_{\text{start}} + \tau_{\text{acc}} \left(\frac{r}{R_s} \right), \quad (3)$$

where t_{start} is the time at which the satellite begins accreting relative to the formation of CAI's and τ_{acc} , which is a free parameter, is the time scale to accrete the fully assembled satellite of radius R_s . Radiogenic heating also depends on the mass fraction of rock in the satellite, m_r , which is related to the uniform rock and ice densities (ρ_r, ρ_i) as

$$m_r = \frac{\rho_r (\bar{\rho} - \rho_i)}{\bar{\rho} (\rho_r - \rho_i)}. \quad (4)$$

Values of ρ_r and ρ_i assumed for each satellite are summarized in Table 2. For Callisto, we construct simple interior models by assuming a constant ice and rock density as a function of depth, $\rho_r = 3000$ kg m⁻³, midway between values for Prinn/Fegley rock ($\rho_r \sim 3300$ kg m⁻³) and CI chondrite ($\rho_r \sim 2800$ kg m⁻³), which are two models for the composition of the satellites' rocky components used by Mueller and McKinnon (1988), and $\rho_i = 1400$ kg m⁻³, representative of the compressed densities of the various ice phases in Callisto's deep interior (including ice I at the surface, and layers of ice III, V, VI, and VII at depth). Because the accretional temperature profile is a strong function of the rock mass fraction, the ice density for Callisto has been chosen so that m_r in our simple uniform-density model is equal to the value obtained from more detailed structural models (McKinnon, 1997), $m_r = 0.44$. For Rhea, we assume a uniform-density model with $\rho_i = 1000$ kg m⁻³, giving $m_r = 0.28$. The specific heat of the bulk satellite is estimated using the mass-weighted average of the rock specific heat

Table 3
Radiogenic heating

Isotope	MeV decay ⁻¹ ^a	Initial abundance ^b	$q(0)$ (W kg ⁻¹) Cl	λ (yr ⁻¹)	$t_{1/2}$ (yr)
²³⁸ U	47.1	0.01873	1.6×10^{-12}	1.55×10^{-10}	4.46×10^9
²³⁵ U	44.2	0.005918	2.99×10^{-12}	9.84×10^{-10}	7.04×10^8
²³² Th	39.9	0.04399	1.00×10^{-12}	4.95×10^{-11}	1.40×10^{10}
⁴⁰ K → ⁴⁰ Ca	0.52	5.37	1.43×10^{-11c}	4.96×10^{-10}	1.39×10^9
⁴⁰ K → ⁴⁰ Ar	0.16	5.37	6.36×10^{-13c}	5.81×10^{-10}	1.19×10^9
²⁶ Al	3.3	84100	1.82×10^{-7d}	9.68×10^{-7}	7.16×10^5
⁶⁰ Fe	0.502	768900 (⁵⁶ Fe)	$(1.34 \pm 0.76) \times 10^{-9e}$	4.26×10^{-7}	1.5×10^6

^a Values from Urey (1955).

^b Atoms per 10⁶ atoms Si; $106,500 \times 10^{-6}$ g Si/g Cl (Lodders, 2003).

^c ⁴⁰K → ⁴⁰Ca with 89% probability, and ⁴⁰K → ⁴⁰Ar with 11% probability.

^d Initial Solar System ²⁶Al/²⁷Al = 5.85×10^{-5} (Thrane et al., 2006).

^e Initial Solar System ⁶⁰Fe/⁵⁶Fe = $(1.9 \pm 0.9) \times 10^{-7}$ (Tachibana and Huss, 2003; Mostefaoui et al., 2004).

$C_{p,r} \sim 700$ J kg⁻¹ K⁻¹ and ice specific heat $C_{p,i} = 2100$ J kg⁻¹ K⁻¹, with $C_p = m_r C_{p,r} + (1 - m_r) C_{p,i}$, which gives $C_p = 1480$ J kg⁻¹ K⁻¹ for Callisto and $C_p = 1700$ J kg⁻¹ K⁻¹ for Rhea.

Table 3 summarizes radiogenic heating rates in CI chondrite in the early Solar System. We consider ²⁶Al as the primary heat source in the early histories of Rhea and Callisto because it provides a factor of 100× more heat than other short-lived isotopes such as ⁶⁰Fe. Long-lived isotopes are not important heat sources during accretion. Aluminum-26 heating is particularly effective at melting bodies early in their histories because of its high elemental abundance in rock, and because its heat is delivered quickly—faster than it can be removed by conduction and possible convection. We estimate the ²⁶Al heating rates for the satellites' rocky components using CI elemental abundances from Lodders (2003). The initial Solar System ²⁶Al/²⁷Al ratio and its spatial heterogeneity is an area of active research. The value is commonly assumed to be homogeneous within the Solar System and between ~ 5 to 7×10^{-5} (Bizzarro et al., 2004, 2005; Thrane et al., 2006; Wadhwa et al., 2007). We adopt an initial Solar System ²⁶Al/²⁷Al = 5.85×10^{-5} (Thrane et al., 2006) appropriate for carbonaceous chondrites, and in the middle of measured values from various meteorite types. If $t = 0$ corresponds to CAI formation, the initial heating rate from ²⁶Al is $q_{26}(0) = 1.82 \times 10^{-7}$ W kg⁻¹, which is a factor of 10⁵ higher than present chondritic values from long-lived isotopes (Spohn and Schubert, 2003). The heating rate decays as $\exp(-\lambda_{26}t)$ with $\lambda_{26} = 9.68 \times 10^{-7}$ yr⁻¹, which corresponds to a half life of 0.716 Myr.

In our model, after material at a radius r is accreted onto the satellite with its temperature $T(r)$ determined by Eq. (1), radiogenic heating increases its temperature by an amount ΔT_r ,

$$\begin{aligned} \Delta T_r(r, t) &= \frac{1}{C_p} \int_{t_f(r)}^t m_r q_{26}(t) dt \\ &= \frac{m_r q_{26}(0)}{C_p \lambda_{26}} [\exp(-\lambda_{26} t_f(r)) - \exp(-\lambda_{26} t)], \end{aligned} \quad (5)$$

where $t_f(r)$ is the formation time of a given layer at radius r relative to CAI's (given by Eq. (3)). At every time step, a layer is added to the satellite, and $T(r) + \Delta T_r(r, t)$ is calculated for all $r < r_{\max}(t)$, where r_{\max} is the radius of the outermost layer of the satellite at time t . Solutions of Eqs. (1) and (5) give time-dependent accretional temperature profiles within the growing satellite. For example, Fig. 2 illustrates time-dependent temperature profiles in a model Callisto that accretes in $\tau_{\text{acc}} = 0.4$ Myr and starts accretion $t_{\text{start}} = 2.5$ Myr after CAI's. Because $T(r) + \Delta T_r(r, t) > T_m$ when the satellite has grown to a radius of 2000 km, this is considered to be an unsuccessful model.

Temperatures for $r < r_{\max}$ are compared to the ice phase diagram at every time step, to assess whether the satellite melts

while it accretes. The liquidus temperature of mixtures of ice I and ammonia are determined using (Leliwa-Kopystyński et al., 2002)

$$T_m(P, X) \approx T_0 + AP + BP^2 - CX - DX^2, \quad (6)$$

where T_0 , A , and B are coefficients for the solidus curve for pure water ice (see Table 4), X ($0 \leq X \leq 1$) is the ammonia concentration by mass, $C = 53.8$, and $D = 650$. The melting point of a 30% NH₃–water ice mixture ($X = 0.3$) ranges from 198 K at Rhea's surface to 186 K in Rhea's core. Phase behavior of ammonia–water mixtures at high pressures is not well-constrained, so we are limited to considering the effect of melting due to the presence of NH₃ in the outer layers of the satellites only. The pressure-dependent melting curve for the high-pressure phases of water ice are calculated using Eq. (6) with $X = 0$. Data from Hobbs (1974) were used to determine A and if appropriate, B , for ice III, V, VI, and VII. The pressure P is calculated assuming the unmelted satellite has a uniform density,

$$P(r, t) = \frac{2\pi}{3} G \bar{\rho}^2 (r_{\max}^2(t) - r^2). \quad (7)$$

The pressure at a given location within the satellite will increase over time as the satellite grows.

Because solid-state convection and thermal diffusion are ineffective at removing heat from the satellites' interiors over the lifetime of ²⁶Al, we consider it likely that all ²⁶Al heat will be retained. Although a satellite may remain unmelted while forming, it may still melt if ²⁶Al heating warms it above its melting point before convection and diffusion can cool the satellite. We compute its final temperature profile by adding the full complement of ²⁶Al heating possible,

$$\Delta T_{r, \text{final}}(r) = \frac{1}{C_p} \int_{t_f(R_s)}^{\infty} m_r q_{26}(t) dt = \frac{m_r q_{26}(0)}{C_p \lambda_{26}} \exp(-\lambda_{26} t_f), \quad (8)$$

and check for melting by comparing $T(r) + \Delta T_r(r, \tau_{\text{acc}}) + \Delta T_{r, \text{final}}(r)$ to the pressure-dependent melting curves in the fully assembled satellite (see the bottom right panel of Fig. 2).

5. Results

Accretional temperature profiles depend on three key parameters: the accretion time scale, τ_{acc} , the protosatellite disk temperature T_d , and the start time relative to CAI condensation, t_{start} . For a given τ_{acc} and T_d , there exists a critical start time $t_{\text{start},c}$: satellites that form earlier than $t_{\text{start},c}$ are excessively melted, but satellites forming later than $t_{\text{start},c}$ remain unmelted to the extent needed for consistency with their moment of inertia constraints (see Section 3). The satellite finishes forming at $t_{\text{end},c} = t_{\text{start},c} + \tau_{\text{acc}}$. Estimates of $t_{\text{end},c}$ are used to constrain the earliest time at which an unmelted satellite could form, and in the context of the Canup and Ward model, the earliest time at which gas inflow to the parent planet ends.

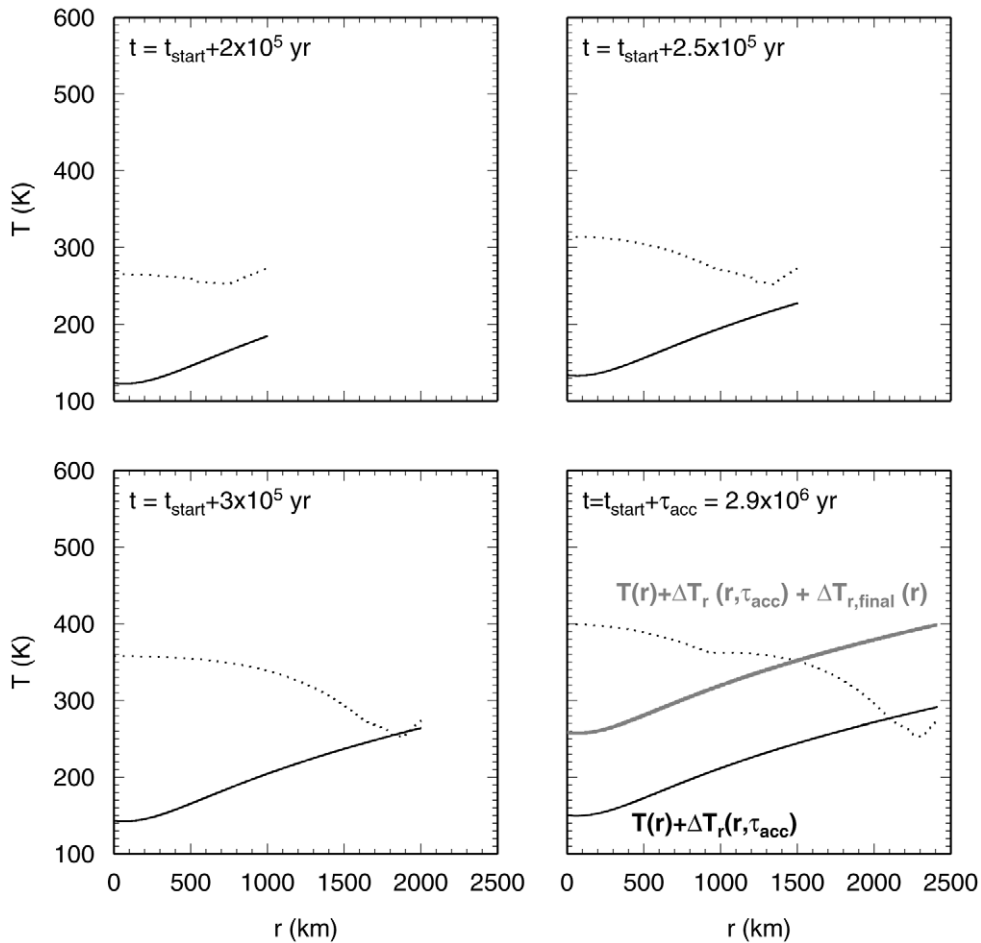


Fig. 2. Time-dependent accretional temperature profiles for Callisto $T(r) + \Delta T_r(r, t)$ (black) and final temperature profile $T(r) + \Delta T_r(r, \tau_{\text{acc}}) + \Delta T_{r,\text{final}}(r)$, accounting for all ^{26}Al heating after accretion ends (gray) for $T_d = 100$ K, $\tau_{\text{acc}} = 0.4$ Myr, and $t_{\text{start}} = 2.5$ Myr. Time-dependent temperature profiles 0.2 Myr into accretion, when the radius of protocallisto is 1000 km (top, left), 0.25 Myr into accretion, when the satellite has grown to 1500 km (top, right), 0.3 Myr when its radius is 2000 km (bottom, left), and $t = t_{\text{start}} + \tau_{\text{acc}} = 2.9$ Myr after CAI's, when Callisto has finished forming (bottom, right). To avoid melting during formation, the temperature profile must always stay below the pressure-dependent melting curves for water ice (dotted lines), even when the maximum amount of ^{26}Al heating is included, as in the final temperature profile (gray line in bottom right panel).

Table 4
Ice properties

Ice phase	Pressure range	T_o (K)	A (K Pa^{-1})	B (K Pa^{-2})
Ice I	$P \leq 209$ MPa	273.2	-7.95×10^{-8}	-9.6×10^{-17}
Ice III	$209 \text{ MPa} < P < 344 \text{ MPa}$	247.7	2.38×10^{-8}	0
Ice V	$344 \text{ MPa} < P < 626 \text{ MPa}$	242.5	4.9×10^{-8}	0
Ice VI	$626 \text{ MPa} < P < 2150 \text{ MPa}$	190.3	1.54×10^{-7}	-3.43×10^{-17}
Ice VII	$P > 2240 \text{ MPa}$	149.9	9.14×10^{-8}	0

5.1. Keeping Rhea unmelted

Fig. 3 shows example accretional temperature profiles for $T_d = 95$ K. In a very slowly accreting Rhea ($\tau_{\text{acc}} = 1$ Myr), the interior of the satellite is warmer than the surface because energy lost due to radiative cooling exceeds the accretional energy flux. For shorter accretion time scales, the accretional energy flux is larger, leading to satellites with surfaces that are warmer than their deep interiors. If Rhea forms in $\tau_{\text{acc}} = 1000$ yr, surface temperatures are above the melting point of ice, unless accretion is delayed until $t_{\text{start}} > 2.5$ Myr after CAI formation for $T_d = 95$ K.

Fig. 4 illustrates how the critical end time $t_{\text{end},c} = t_{\text{start},c} + \tau_{\text{acc}}$ for Rhea varies as a function of T_d , τ_{acc} , and ammonia abundance. Given the constraints on accretional melting from *less et al. (2007)* ($z_{\text{ice}} \leq 158$ km), Rhea must finish accreting *no earlier* than 1.9 Myr after CAI formation, obtained for the coldest disk tem-

perature $T_d = 70$ K. For a warm disk with $T_d = 160$ K, and fast accretion time, $\tau_{\text{acc}} = 10^3$ yr, Rhea must complete its formation no earlier than 3.8 Myr after CAI formation. For $\tau_{\text{acc}} \leq 10^3$ yr, and $T_d > 190$ K, melting occurs even without radiogenic heating. The constraint on $z_{\text{ice}} \leq 46$ km from *Anderson and Schubert (2007)* requires cooler disk temperatures, later t_{end} , and longer τ_{acc} . For $z_{\text{ice}} \leq 46$ km, Rhea must still finish accretion no earlier than 1.9 to 7 Myr, but fast accretion ($\tau_{\text{acc}} = 10^3$ yr) in this scenario requires a cooler disk ($T_d \leq 155$ K).

If Rhea contains 30% NH_3 (close to the maximum NH_3 abundance; see *Schubert et al., 1986*), it must have finished accreting $2.5 \text{ Myr} < t_{\text{end},c} < 7 \text{ Myr}$ after CAI's, regardless of the value of z_{ice} . The presence of ammonia in Rhea requires low disk temperatures, $T_d < 185$ K, essentially below the melting point of a 30% NH_3 - H_2O mixture, even if the satellite forms slowly. Fast accretion with 30% NH_3 leads to excessive melting in most cases.

5.2. Keeping Callisto unmelted

Fig. 5 illustrates how the final accretional temperature profiles for Callisto depend on t_{start} and τ_{acc} for $T_d = 100$ K. Callistos with accretion time scales $\ll 1$ Myr suffer complete ice melting. Callistos that accrete in ≤ 1 Myr are heated principally at their surfaces by impacts so $dT(r)/dr \geq 0$ throughout most of their interiors, while very slow accretion times ($\tau_{\text{acc}} \geq 3$ Myr) yield cases that

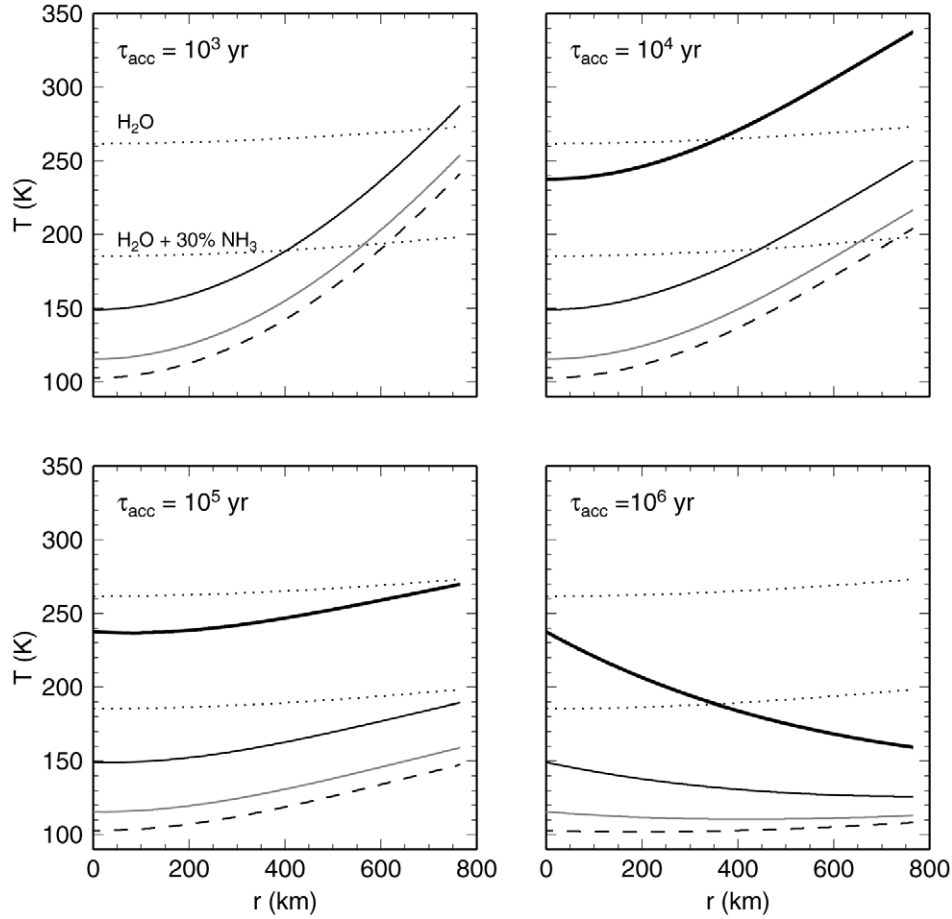


Fig. 3. Final accretional temperature profiles ($T(r) + \Delta T_r(r, \tau_{\text{acc}}) + \Delta T_{r,\text{final}}(r)$) for Rhea with $T_d = 95$ K, $t_{\text{start}} = 2$ Myr (bold black), 3 Myr (solid black), 4 Myr (gray), and 5 Myr (dashed) after CAI formation. If Rhea forms in 1000 yr (top, left) it is heated principally by impacts leading to a warm surface and cool interior. If Rhea forms in $\tau_{\text{acc}} = 1$ Myr (bottom, right) it is heated principally by ^{26}Al decay and is warm inside and cold at its surface. Melting temperatures of pure water ice I (upper dotted line) range from 273 to 260 K. The pressure-dependent melting point of a 30% $\text{NH}_3\text{-H}_2\text{O}$ mixture (185 to 200 K) is shown by the lower dotted line.

are heated primarily by ^{26}Al and have relatively warm interiors ($T \sim 200\text{--}350$ K) and cold surfaces $T \sim T_d$. This may facilitate the rapid onset of convection post-accretion and prevent Callisto from melting during the first 500 Myr of its thermal evolution.

In order for Callisto to avoid melting during formation, it must form in $\tau_{\text{acc}} \geq 0.6$ Myr. This can be obtained by solving Eq. (1) in the absence of radiogenic heating for τ_{acc} ,

$$\tau_{\text{acc,min}} = \frac{\bar{\rho}r \left[\frac{4\pi}{3} \frac{F_g}{(F_g - 1)} \bar{\rho}Gr^2 - C_p(T - T_d) \right]}{3\sigma_{\text{SB}}(T^4 - T_d^4)}. \quad (9)$$

The requirement that $T = 253$ K at a depth of 100 km ($r = 2310$ km), the location of the minimum melting point for water ice, gives $\tau_{\text{acc,min}} = 0.6$ Myr for a nominal $T_d = 100$ K and $F_g = 5$. The requirement that Callisto avoid global melting due to short-lived radioisotope heating alone suggests that Callisto must finish forming *no earlier* than ~ 2.6 to 3 Myr (McKinnon, 2006b).

Fig. 6 illustrates the required end time for Callisto's formation as a function of τ_{acc} and T_d , based on calculations using Eqs. (1) and (5), and (8). When both accretional and radiogenic heating are considered together, we find that a model Callisto forming in a disk with $70 \text{ K} \leq T_d \leq 165 \text{ K}$ must finish forming *no earlier* than 3.9 Myr after CAI condensation to avoid melting. In a warm disk with $T_d = 160$ K at Callisto's location, the satellite must finish forming no earlier than 4.4 Myr after CAI condensation to avoid melting.

During most of Callisto's accretion when $u_i > 0.8 \text{ km s}^{-1}$, the specific impact energy exceeds the latent heat of fusion of water

ice. This suggests that the ice components of impactors will melt during accretion. In our calculations we require that impactors are small enough to deposit heat at depths shallow enough for efficient radiative cooling. Therefore, release of rock from impactors during accretion should not significantly affect the overall rock distribution in the outer layers of the satellite. We note that the fate of rock released from satellitesimals will be important for driving early differentiation dynamics and should be considered in future work.

5.3. Presence of ammonia in Callisto

Galileo magnetometer results indicate that Callisto shows an inductive response to the apparent time-variable jovian magnetic field (Zimmer et al., 2000). This suggests that Callisto has a liquid water ocean underneath its outer layers of solid ice. In order for Callisto's ocean to remain thermodynamically stable over time, the heat flux from its interior must exceed the conductive (and possibly convective) heat flux across its ice shells. Because it is likely that Callisto's outer ice shell is thick enough to convect (Spohn and Schubert, 2003; McKinnon, 2006a), convection should remove enough of the radiogenic heat from its interior to cause the ocean to freeze (Spohn and Schubert, 2003). It has been suggested that if Callisto's ice shell contained 5% NH_3 by weight, a subsurface liquid water ocean can remain in thermodynamic steady state against heat transport by solid-state convection (Spohn and Schubert, 2003). [Other materials such as sulfate salts,

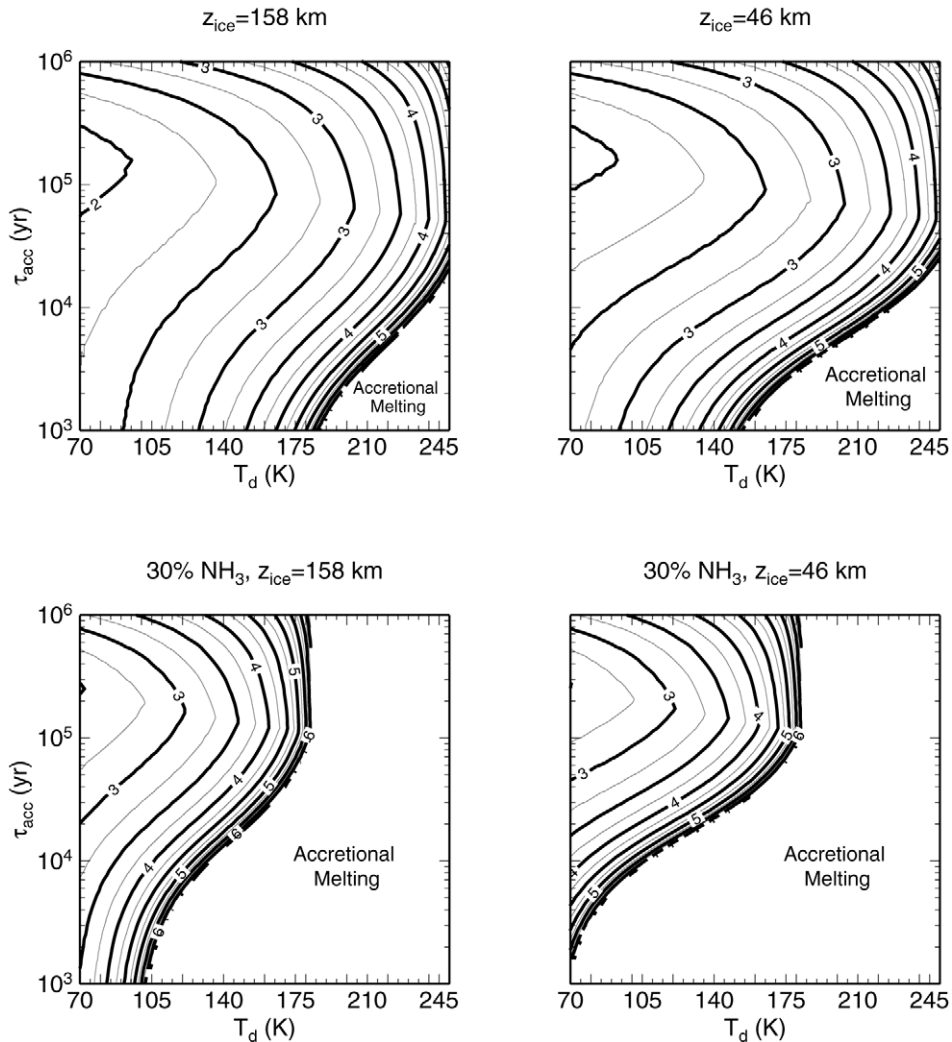


Fig. 4. Contours of $t_{\text{end},c}$ required to prevent Rhea from melting during its formation as a function of τ_{acc} and T_d . For a given τ_{acc} and T_d , contours represent the *earliest* possible time of the completion of Rhea's accretion. Fast accretion and high T_d leads to near-surface melting and yields accretional temperature profiles with more melting than permitted by its measured moment of inertia constraints (gray regions). (Top, left) Required t_{end} for Rhea, assuming a pure water ice composition and the less et al. (2007) moment of inertia constant, which implies a $z_{\text{ice}} = 158$ km-thick rock-free layer at Rhea's surface. (Top, right) Pure water ice composition and $z_{\text{ice}} = 46$ km (implied by Anderson and Schubert, 2007). (Bottom, left) Required t_{end} for $z_{\text{ice}} = 158$ km and 30% NH_3 by mass. (Bottom, right) Required t_{end} for $z_{\text{ice}} = 46$ km and 30% NH_3 .

which may be present in Europa's ice shell due to water-rock chemistry (McKinnon and Zolensky, 2003), can lower the melting point of the ocean, as well.] Although NH_3 may help explain the current presence of an ocean, is it compatible with formation of an unmelted Callisto?

A $\text{H}_2\text{O}-\text{NH}_3$ mixture that is 5% NH_3 by weight has a minimum melting temperature of 248 K at a pressure of 209 MPa (Leliwa-Kopystyński et al., 2002). In our model Callistos, this corresponds to a depth of 100 km. Using Eq. (9), we impose the limit that the interior temperature $T \leq 248$ K at $r = 2310$ km, and solve for the required τ_{acc} to keep an ammonia-rich Callisto unmelted. We find that $\tau_{\text{acc}} > 0.7$ Myr for $T_d = 100$ K. Uncertainties in the liquidus temperature of $\text{H}_2\text{O}-\text{NH}_3$ mixtures at the high pressures associated with Callisto's deep interior prevents us from placing tighter limits on the start time of accretion of an ammonia-water Callisto. However, because the melting temperature of the water/ammonia mixture is not much lower than pure water ice, it is likely that the constraints on t_{start} for the water/ammonia case will be similar to those for the pure water case. This implies that up to 5% NH_3 its ocean is consistent with the formation of an initially undifferentiated Callisto provided it accreted in $\tau_{\text{acc}} > 0.7$ Myr.

5.4. Fate of Ganymede

Despite their similarities in size and mean density, Ganymede and Callisto have remarkably different surfaces and interior structures. Two-thirds of Ganymede's surface is covered with bright "grooved terrain" consisting of lanes of parallel grooves formed by intense lithospheric deformation, interred to be evidence of a past epoch of endogenic activity driven by tides and interior fluid motions (Kirk and Stevenson, 1987; Showman and Malhotra, 1997). Magnetic field measurements in the vicinity of Ganymede suggest that it has an intrinsic dipole magnetic field, perhaps evidence of a metallic core (Schubert et al., 1996). Ganymede's moment of inertia constant is consistent with a fully differentiated interior with a metal core, rock mantle, a thick mantle of high-pressure water ice phases, a liquid water ocean, and an outer layer of water ice I (Schubert et al., 2004).

Several causes for the differences between these satellites have been proposed. It is possible that the dichotomy is primordial, resulting from differences in the retention of accretional heat (Schubert et al., 1981), differences in accretional time scales (Mosqueira and Estrada, 2003), differing nebular temperatures (Stevenson et al., 1986), and/or differing roles of atmospheric

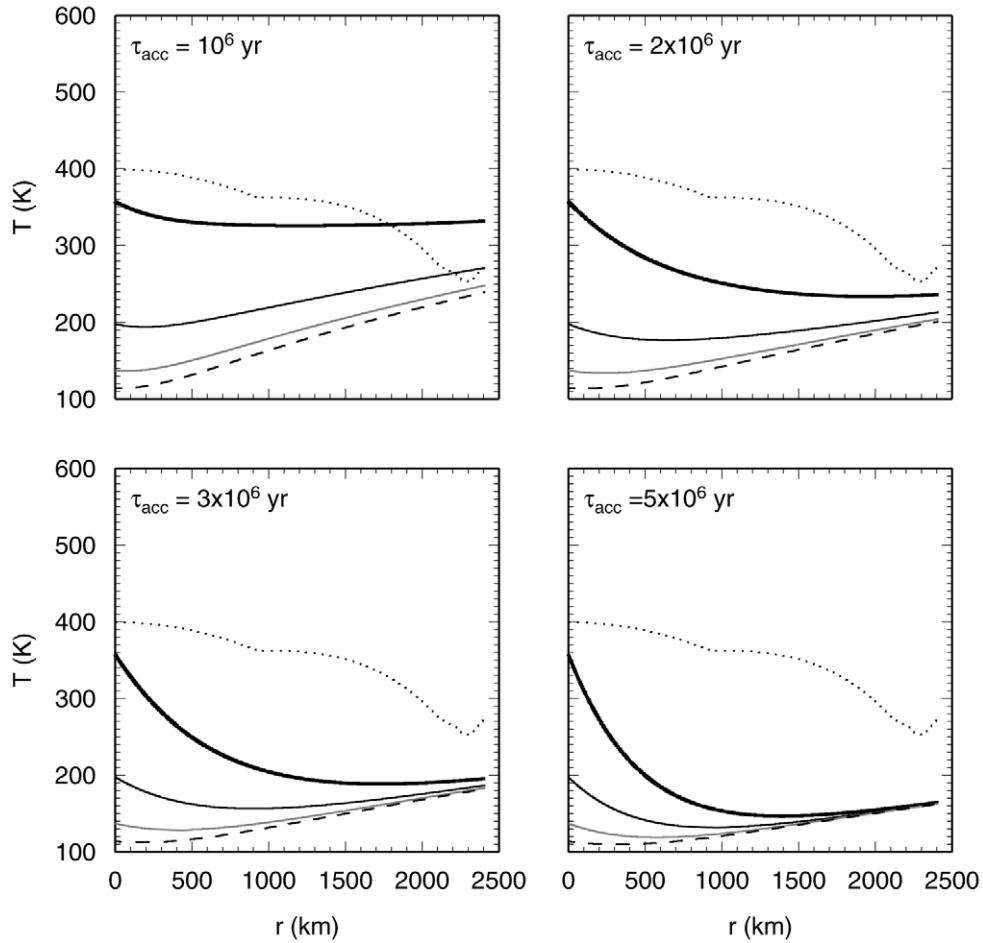


Fig. 5. Final accretional temperature profiles for Callisto $T(r) + \Delta T_r(r, \tau_{\text{acc}}) + \Delta T_{r,\text{final}}(r)$ for $T_d = 100$ K, for $\tau_{\text{acc}} = 1$ Myr (top, left), 2 Myr (top, right), $\tau_{\text{acc}} = 3$ Myr (bottom, left), and $\tau_{\text{acc}} = 5$ Myr (bottom, right), starting 2 Myr after CAI's (bold lines), 3 Myr (thin solid), 4 Myr (gray), and 5 Myr (dashed). The pressure-dependent melting curves of water ice are shown in the dotted lines.

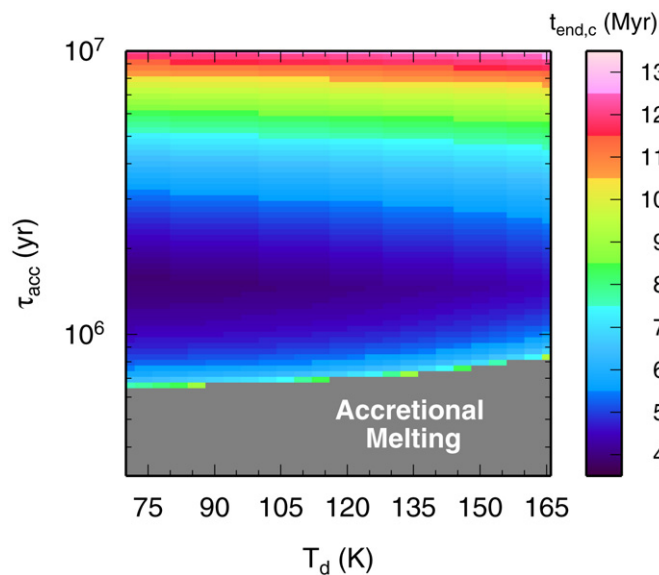


Fig. 6. Required t_{end} for Callisto to remain unmelted as a function of the accretion time (τ_{acc}) and nebular temperature (T_d) (similar to Fig. 4). In the absence of radiogenic heating, for accretion times less than ~ 0.6 Myr, Callisto melts during its formation. If Callisto finishes accreting earlier than 3.9 Myr after CAI's, it will melt during formation or immediately thereafter due to decay of ^{26}Al in its interior.

drag in planetesimal breakup (Lunine and Stevenson, 1982). It is also possible that both satellites formed undifferentiated but followed different evolutionary pathways, with Ganymede receiving more heat from radiogenic decay (Friedson and Stevenson, 1983; Mueller and McKinnon, 1988) and tidal heating during resonance passages (Showman and Malhotra, 1997).

Because Ganymede is larger, has more rock than Callisto, and is closer to Jupiter in the protosatellite disk, we expect that the accretional temperature profiles in Ganymede will be somewhat warmer. In the CW model, Ganymede and Callisto would form with similar τ_{acc} . To evaluate whether the differences between Ganymede and Callisto could be due to differences in their accretional environments, we determine time-dependent accretional profiles for Ganymede using values of τ_{acc} and t_{start} that resulted in unmelted callistos. For a disk temperature of 100 K at Callisto's orbital radius and $140 \text{ K} \leq T_G \leq 180 \text{ K}$ at Ganymede, Fig. 7 shows conditions in which Callisto is unmelted while Ganymede melts (white regions). The region of parameter space that produces a primordial dichotomy grows as the difference in disk temperatures is increased. We find that accretion times on the low end of those consistent with an unmelted Callisto and early start times favor melted ganymedes, consistent with a primordial dichotomy.

6. Discussion

Partially differentiated satellites provide a unique opportunity to constrain the timing and duration of their formation. To avoid complete ice/rock separation, partially differentiated satellites must

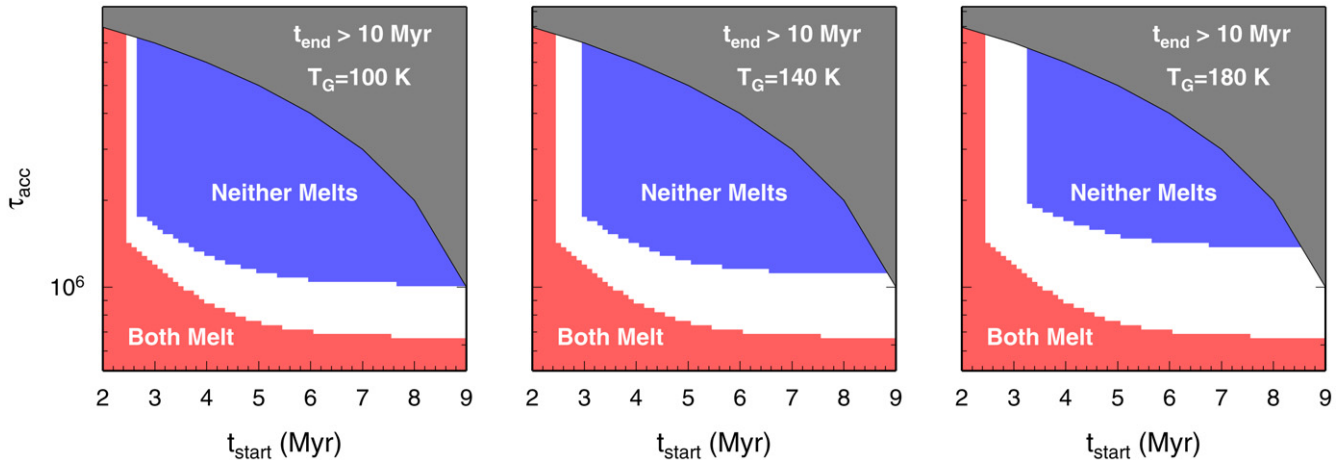


Fig. 7. Fates of Ganymede and Callisto as a function of accretional timescale, start time relative to CAI condensation, and disk temperature at Ganymede, T_G . We assume T_d at Callisto is 100 K, and a range of values for T_G constrained by the difference in temperature at Ganymede and Callisto's locations during the time of Galilean satellite formation from Fig. 1. We consider end times greater than 10 Myr to be unphysically long because they exceed likely nebular lifetimes, which defines unpermitted combinations of τ_{acc} and t_{start} (gray region). If $T_G = 100$ K (left), neither satellite melts (blue) if accretion begins more than 2.4 Myr after CAI's and the satellite accretes in $\tau_{\text{acc}} \gtrsim 1$ Myr. Regions in which Ganymede melts but Callisto does not are white. The likelihood of a primordial dichotomy increases as the disk temperature at Ganymede increases from $T_G = 140$ K (middle) to $T_G = 180$ K (right).

avoid widespread melting during their entire histories, including during formation, when their surfaces would have been heated by impacts and interiors heated by short-lived ^{26}Al . By calculating accretional temperature profiles for two candidate partially differentiated satellites, Callisto and Rhea, we have placed constraints on the timing and duration of each satellite's accretion.

If Callisto was assembled from small planetesimals that deposit their impact energy close to the surface where it can be lost by radiative cooling, it can avoid melting if it formed on a time scale longer than 0.6 Myr. Considering both ^{26}Al and accretional heating, Callisto must finish forming no earlier than ~ 4 Myr after CAI's. The possible presence of 5% NH_3 , which lowers the minimum melting point of the ice mixture to 248 K and enhances the thermodynamic stability of its present-day ocean (Spohn and Schubert, 2003) is compatible with a partially differentiated Callisto formed in $\tau_{\text{acc}} > 0.7$ Myr. Saturn's satellite Rhea must have finished accreting no earlier than 1.9 Myr after CAI condensation to avoid early melting. In the case of rapid formation ($\tau_{\text{acc}} \leq 10^3$ yr), Rhea's formation must have been delayed until at least 2.6 Myr after CAI's if the disk temperature is ≈ 70 K; if $T_d = 120$ K, formation must be delayed until 3.6 Myr after CAI's. For $\tau_{\text{acc}} \leq 1000$ yr and $T_d \gtrsim 155$ K to 190 K, Rhea melts in excess of that implied by current moment of inertia estimates. If Rhea has 30% NH_3 , its accretion must end *no earlier* than 2.5 Myr after CAI condensation and occur in a disk with $T_d < 185$ K to avoid excessive melting.

Considering timing constraints at both Jupiter and Saturn implies that gas giant satellite formation ended *no earlier* than ~ 4 Myr after CAI's. It is likely that the saturnian satellites formed at the same time as, or later than Jupiter's, which suggests that Rhea's interior (and by extension, the interiors of the other inner saturnian satellites Mimas, Enceladus, Tethys, and Dione), would not have experienced much ^{26}Al heating. By 4 Myr after CAI condensation, the ^{26}Al heating rate has decayed to 2% of its initial value, or $\sim 10^{-9}$ W kg^{-1} of CI. The temperature rise due to ^{26}Al in the interior of an icy satellite with 30% rock would be limited to $O(10)$ K. This places constraints on the amount of activity driven by early heating in the Saturn system (Castillo-Rogez et al., 2007).

Satellites and/or the material that comprises them may migrate inward in orbital radius as the satellites form. If such migration is significant, disk and impactor temperatures lower than those estimated for the current satellite locations (e.g., Fig. 1) would apply. The satellite accretion simulations of Canup and Ward (2006) demonstrate that in the presence of ongoing inflow to the disk,

satellite orbits spiral inward via Type I migration (e.g., Ward, 1997) once they exceed a critical mass. As long as the inflow continues, a decaying satellite (and entire satellite systems) will ultimately be lost to collision with the planet. The satellite systems we see today are those that avoid this fate by forming as the inflow ended and the circumplanetary disk dissipated. In the Canup and Ward (2006) simulations that produced Jupiter-like systems, the Callisto analogs migrated inward in semi-major axis by less than $\lesssim 5$ planetary radii before the inflow ended and Type I migration ceased (e.g., their Fig. 3). Their predicted disk temperatures do not change much across this scale of orbital radius (see Fig. 1). In their Saturn-like systems, Canup and Ward (2006) find that the small- to medium-sized inner satellites do not migrate substantially, because they are too small for Type I migration to be important. In the Mosqueira and Estrada (2003) model, the solids that accrete into Rhea may have initially been located outside Rhea's current orbit (I. Mosqueira, personal communication), while the planetesimals that accrete into Callisto are predicted to originate at distances as large as $\sim 100R_J$ (Mosqueira and Estrada, 2003).

Here we have calculated accretional temperature profiles for Callisto and Rhea in the limit of maximally efficient cooling, and corresponding to small impactors. This assumption is valid if the satellite is assembled from impactors small enough to deposit their impact energy in a layer of thickness δ_{heat} , which is thinner than or comparable to the depth, δ_{cool} , to which the satellite cools conductively in the time it takes the satellite to accrete an additional layer of thickness δ_{heat} , $\sim \delta_{\text{heat}}(dr/dt)^{-1}$. Simulations and experiments suggest that impact-induced shock heating is deposited in a near-surface layer $\delta_{\text{heat}} \sim 3$ to 5 times the impactor radius in impacts with $u_i \sim 5$ to 10 km s^{-1} (Gault and Heitowitz, 1963; O'Keefe and Ahrens, 1982; Squyres et al., 1988). Numerical impact simulations show that for a given impactor size, the depth of heat deposition of shock heating is proportional to impact velocity (e.g., Pierazzo et al., 1997), so impacts with $u_i \sim 1$ to 3 km s^{-1} should have δ_{heat} comparable to the impactor radius. The thickness of the near-surface boundary layer that cools conductively is $\delta_{\text{cool}} \sim \kappa(dr/dt)^{-1}$, with $\kappa \sim 2 \times 10^{-6}$ $\text{m}^2 \text{s}^{-1}$ for ice and $dr/dt \sim r/(3\tau_{\text{acc}})$. We find that $\delta_{\text{heat}} \lesssim \delta_{\text{cool}}$ for impactors with radii $r_{\text{par}} \lesssim 10^2$ m ($\tau_{\text{acc}}/10^6$ yr)(1000 km/r). For $\tau_{\text{acc}} \sim 10^6$ yr, these critical impactor sizes are larger than the characteristic sizes of objects predicted to accrete onto Rhea and Ganymede in the CW model, but smaller than the maximum values predicted for objects impacting Callisto (\lesssim km-sized, see Appendix B). Thus, $\eta \sim 0$

should be a good approximation for Rhea and Ganymede, but may underestimate accretional heating in Callisto in the CW model. Even larger impactors may be appropriate to other scenarios. For example, Mosqueira and Estrada (2003) propose that Callisto was assembled from 300 to 500 km-scale objects, although this estimate did not include the potential effects of fragmentation (I. Mosqueira, personal communication). Retention of accretional energy associated with larger impactors as a function of depth will result in warmer predicted temperature profiles for a given set of nebular conditions, and will lead to longer required accretion times and/or later required end times for accretion.

Our calculations do not consider the formation of atmospheres on growing model callistos or rheas. We do not expect an impact-generated atmosphere to form on either body, because the impacts that form both satellites have characteristic velocities too low to generate shock-induced vapor. Complete vaporization of ice, which would be required to form a substantial atmosphere, occurs for $u_i > 10 \text{ km s}^{-1}$ (Pierazzo et al., 1997), but the maximum u_i expected on Rhea and Callisto are only ~ 1 to 3 km s^{-1} . Large icy satellites such as Callisto with $M > 10^{22} \text{ kg}$ have escape velocities that exceed the likely sound speed in the disk's gas, and as a result, the gas density in the satellite's Hill sphere can exceed that in the disk as a whole (Lunine and Stevenson, 1982). The formation of such an atmosphere makes it extremely difficult to prevent Callisto from melting (Stevenson et al., 1986). Inclusion of this effect and re-evaluation of the likelihood that Callisto accretes a gaseous envelope that "blankets" its surface during accretion is a subject of future work.

Although our calculations suggest that Callisto can avoid melting and differentiation during formation, the early differentiation dynamics in a homogeneous Callisto and its long-term thermal evolution as a partially differentiated body remain somewhat mysterious. After Callisto's formation, its interior will be heated by long-lived radioisotopes present in the co-accreted rock. As recognized by Friedson and Stevenson (1983), this heat must be removed from its interior by efficient solid-state convection, otherwise Callisto will warm to close to its melting point and begin to differentiate. However, even a small increase in rock fraction as a function of depth would inhibit solid-state convection because thermal buoyancy perturbations that drive shell convection would be overwhelmed by the increase in bulk satellite density. The end result would be a gravitationally stable ice-rock mantle that would be unable to remove heat liberated by downward sinking rock particles and radiogenic heating. Without convection, differentiation of Callisto would be driven to completion.

7. Summary

For reasonable accretion conditions, we find that both Rhea and Callisto can avoid melting in excess of that consistent with their present moment of inertia values during their formation. Rhea can remain unmelted even if it formed rapidly provided disk temperatures are cold enough, and it finishes forming late enough to avoid melting by ^{26}Al heating ($\sim 2 \text{ Myr}$ after CAI's). Expanding on prior predictions (Stevenson et al., 1986), we find that Callisto must form slowly, in $\tau_{\text{acc}} > 0.6 \text{ Myr}$ (for a nominal $T_d = 100 \text{ K}$), to avoid global melting during accretion in the limit of small impactors. If Callisto is warmed by both accretional and radiogenic heating, it must finish forming no earlier than $\sim 4 \text{ Myr}$ after CAI's to avoid melting and differentiation during accretion. The same accretion start times and time scales that give undifferentiated callistos can be consistent with melted ganymedes and a primordial origin for the satellites' differing interior structures.

Our accretional temperature profiles are calculated in the limit of maximally efficient cooling, in the limit of small impactors ($h \sim 0$). Large, differentiated impactors are likely particularly prob-

lematic for Callisto because intact rock fragments larger than a few km can sink to its center during accretion, potentially triggering differentiation. Any retention of heat at depth and/or satellite assembly from larger objects will yield warmer temperature profiles and more restrictive constraints on the satellites formation environments than those given here.

Because Callisto is a much larger object than Rhea, and the energy associated with its assembly is much higher, the requirement that Callisto remain unmelted provides much more restrictive constraints on the timing of satellite formation and solar nebula disk dispersal. If Saturn formed at the same time as, or soon after Jupiter, the requirement that Callisto remain unmelted during formation implies that satellite formation at both Jupiter and Saturn ended no earlier than $\sim 4 \text{ Myr}$ after CAI's. In the context of the CW model, the earliest end time for Callisto's accretion implies that the complete removal of the solar nebula occurred no earlier than 4 Myr after CAI's. This is slightly longer than the mean nebular lifetime of 3 Myr inferred in young star clusters based on measurements of excess infrared emission from constituent stars (Haisch et al., 2001; Bouwman et al., 2006). It is also comparable to the time scale needed to form Jupiter in recent calculations involving a $5M_{\oplus}$ core and a reduced envelope opacity (Hubickyj et al., 2005).

Acknowledgments

This work is supported by NASA Outer Planets Research Program grant NNG05GH67G to R.M. Canup. We thank I. Mosqueira, O. Hubickyj, and G. Schubert for their reviews, and W.R. Ward and D.J. Stevenson for helpful discussions.

Appendix A. Midplane disk temperature profiles in the Canup and Ward model

We here describe the method used to estimate mid-plane temperatures in an inflow-supplied protosatellite disk (e.g., the CW curves in Fig. 1). For details, the reader is referred to Canup and Ward (2002, 2006, 2008).

The disk is heated by luminosity from the planet, viscous dissipation, and energy dissipation associated with the difference between the free-fall energy of the incoming gas and that of a Keplerian orbit. These energy sources are balanced by radiative cooling. CW consider an alpha viscosity, with $\nu = \alpha cH \approx \alpha c^2/\Omega$, where α is a constant, c is the gas sound speed, $H \approx c/\Omega$ is the disk's vertical scale height, and $\Omega = (GM_p/a^3)^{1/2}$ is the orbital frequency at radius a in the disk. The equation for thermal balance is (Canup and Ward, 2002)

$$\frac{9}{4} \left[\sigma_{\text{SB}} T_p^4 \left(\frac{R_p}{a} \right)^2 \frac{c}{a\Omega} + \chi \alpha c^2 \sigma_g \right] = 2\sigma_{\text{SB}} (T_{\text{eff}}^4 - T_{\text{neb}}^4), \quad (\text{A.1})$$

where T_p and R_p are the planet's temperature and radius, σ_g is the gas surface density in the disk, $\chi \equiv 1 + \frac{3}{2}[(r_c/a)^2 - (1/5)]^{-1}$ is a term arising from the mass inflow, r_c is the outer radius of the inflow region, T_{neb} is the ambient temperature into which the circumplanetary disk radiates, T_{eff} is the disk's effective temperature, and the factor of 2 on the r.h.s. arises because the disk radiates from both its upper and lower surfaces.

In the CW model, the gas surface density reflects a quasi-steady-state balance between the supply of gas from inflow, and gas removal due to viscous spreading onto the planet or beyond the disk's outer edge. We calculate σ_g using Eq. (18) of Canup and Ward (2002), assuming that the inflow across the disk is uniform, and relate T_{eff} to the disk mid-plane temperature T_d using an expression appropriate in both the high and low optical depth regimes [Eq. (A.15) of Nakamoto and Nakagawa, 1994; see also

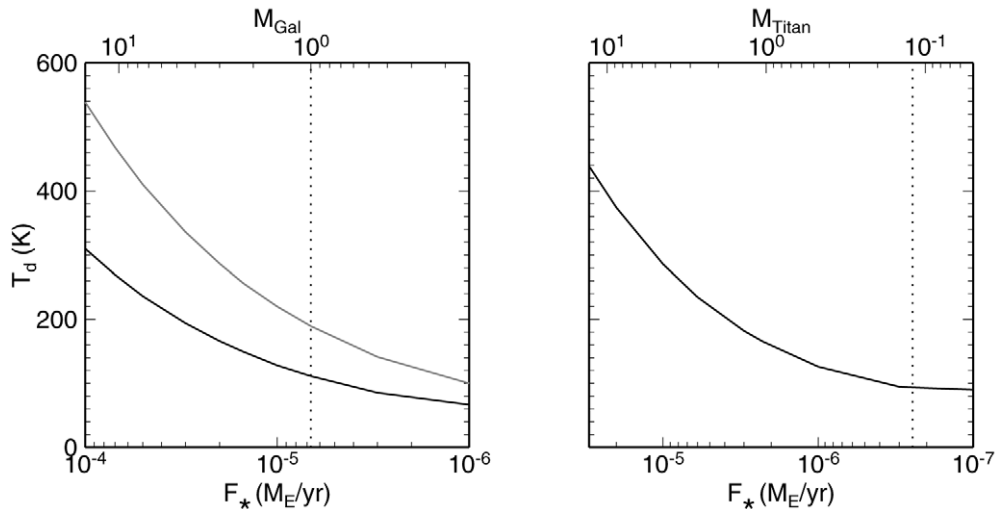


Fig. 8. (Left) Sample midplane temperatures in the Canup and Ward model at the current locations of Ganymede (gray curve) and Callisto (black curve) as a function of the inflow rate of gas and solids to Jupiter in Earth masses (M_E) per year. The top axis is the total remaining mass in solids (scaled to the mass of the Galilean satellites, M_{Gal}) that will be delivered to the disk before the inflow ends as a function of F_* , assuming a solar composition inflow ($f \sim 10^2$) and $\tau_{in} = 10^6$ yr. The dotted line shows the time after which a mass in solids equal to that of the Galilean satellites will be delivered to the disk. (Right) Same as left frame, only for Saturn at the current location of Rhea. Here the dotted line shows the time after which a mass equal to that of the inner saturnian satellites will be delivered to the disk interior to Titan.

Canup and Ward, 2008]. The mid-plane temperature depends on κ_R and κ_B , the disk’s Rosseland and Planck opacities, respectively. Because the CW model invokes the delivery of small particles to the disk with the inflowing gas, an accompanying population of dust and grains appears likely, and in this case, $\kappa_R \sim \kappa_B \sim$ a few $\text{cm}^2 \text{g}^{-1}$ (e.g., Semenov et al., 2003).

The above calculation yields $T_d \propto F_*^{9/20} (\kappa/\alpha)^{1/5}$ when the disk is optically thick (which is true in the regular satellite region when $\kappa_R \sim \kappa_B \sim 1$), and so the disk mid-plane temperature is most strongly affected by the rate of inflow to the disk, F_* (Canup and Ward, 2002, 2008). During runaway gas accretion, inflow rates are predicted to be as high as $\sim 10^{-2}$ Earth masses per year (e.g., Bate et al., 2003), although a jovian planet would probably be too distended at this early time to possess a circumplanetary disk or satellites. Between this early period of rapid inflow and the cessation of gas accretion, the CW model assumes that the inflow to the planet slows, due to depletion of the supply of local gas by the planet and/or the dispersal of the nebula itself. Because T_d is primarily a function of the inflow rate, the disk cools as the rate of inflow to the planet decreases.

Canup and Ward (2006) perform direct simulations of satellite accretion at Jupiter and Saturn, assuming an exponentially decaying inflow with a decay timescale comparable to nebular lifetimes. They find that multiple generations of satellites form and are lost due to inward orbital migration and collision with the planet. In each generation, a satellite system with a similar total mass ($\sim 10^{-4} M_p$) is formed and then lost as another accretes in its place. The surviving satellites are those that form in the last generation as the inflow ends. Both Galilean-like systems with multiple similarly sized satellites and saturnian-like systems in which most of the system mass is in a single satellite (like Titan) can result (Fig. 3 of Canup and Ward, 2006), depending on the timing of the end of inflow relative to the cycles of satellite growth and loss.

Fig. 8 shows the predicted evolution of the midplane temperature in the CW model as a function of inflow rate to Jupiter (left) and Saturn (right) at the current locations of Callisto, Ganymede, and Rhea. All assume $\alpha = 0.006$, background temperature $T_{neb} = 20$ K (appropriate for a planet that has opened a gap in the disk, e.g., D’Angelo et al., 2003), $T_p = 500$ K for Jupiter and T_p for Saturn (e.g., Burrows et al., 1997), and $\kappa_B \sim \kappa_R \sim 1$. For an exponentially decaying inflow with a time constant $\tau_{in} \sim 10^6$ yr, the peak

inflow rates shown in both plots correspond to a time when the planet has acquired approximately 70% of its final mass.

The top axis in both plots shows the total remaining mass in solids that will be delivered to the disk before the inflow ends as a function of F_* , assuming a solar composition inflow ($f \sim 100$) and $\tau_{in} = 10^6$ yr. In the Jupiter plot, the vertical dotted line shows the time after which a mass in solids equal to that of the Galilean satellites will be delivered to the disk. We consider this to be the inflow rate at which the Galilean satellites begin to form, and show the temperature profile at this time in Fig. 1 (left). In the CW model, a Saturn-like system is created when the inflow to the disk ends soon after all large inner satellites (whose masses would have been comparable to that of Titan) have migrated into the planet and been lost (Canup and Ward, 2006). This implies that the current inner saturnian satellites formed last, after the loss of any inner large companions to Titan, and during the very last stages of inflow. In the Saturn plot below, the vertical dotted line shows the time after which a mass in solids equal to that of the inner saturnian satellites will be delivered to the disk within 15 saturnian radii, assuming that the outer edge of the inflow region is $\sim 30R_p$. We consider this to be the inflow rate at which the inner saturnian satellites form, and show temperatures at this time in Fig. 1 (right).

Appendix B. Size estimates for satellitesimals in the Canup and Ward model

Estimates of the sizes of objects accreting onto Callisto and Rhea are key to understanding their post-formation interior states. Here, we estimate the sizes of objects that create each satellite in an inflow-produced gas-starved disk. We estimate particle sizes by assuming a balance between the rate of particle supply to the disk, rate of particle collision with the growing satellite, and rate of collision between particles within the disk. First, we consider the balance between particle supply and loss by collision with the growing satellite. For simplicity we consider a uniform inflow of solids per unit area into the disk between the parent planet’s radius and an outer radial distance r_c . The small particles interact with each other, and with a population of much larger satellites with mass M_s and radius R_s . The large satellites may be thought of as having an effective surface mass density $\sigma_s = M_s/A$, where A

is the area of the annular “feeding zone” of each satellite. The feeding zone area $A = 2\pi a \delta a = 2\pi a^2 C (M_s/3M_p)^{1/3}$, where the radial extent of the feeding zone $\delta a = Ca(M_s/3M_p)^{1/3}$, C is the annulus width in satellite Hill radii, and M_p is the mass of the parent planet.

The small particle population will self-regulate so that the mass rate of particle supply from the inflow to the annulus, $\sim (F_*/f)(A/\pi r_c^2)$, is comparable to the mass removal rate of particles due to collision with the satellite, $\sim \pi R_s^2 \sigma_{\text{par}} \Omega F_g$ where $F_g \equiv (1 + (v_{\text{esc}}/v_\infty)^2)$ is the gravitational focusing factor, and v_{esc} is the escape velocity of the growing satellite. Equating these rates, solving for the small particle surface density σ_{par} , dividing by $\sigma_s = M_s/A$, and setting $F_* = F_*(t_s) = f(M_T/\tau_{\text{in}})$ gives

$$\begin{aligned} \frac{\sigma_{\text{par}}}{\sigma_s} &\sim \left(\frac{F_*(t_s)}{f M_s \Omega} \right) \left(\frac{A}{\pi r_c^2} \right) \left(\frac{A}{\pi R_s^2} \right) \left(\frac{1}{F_g} \right) \\ &\sim \left(\frac{2}{F_g} \right) \left(\frac{M_T}{M_s} \right) \frac{C^2}{\tau_{\text{in}} \Omega} \left(\frac{\rho_s}{\rho_p} \right)^{2/3} \left(\frac{a}{R_p} \right)^2 \left(\frac{a}{r_c} \right)^2 \\ &\sim \left(\frac{1}{F_g} \right) \left(\frac{M_T}{M_s} \right) \frac{1}{(G \rho_p)^{1/2}} \frac{C^2}{\tau_{\text{in}}} \left(\frac{\rho_s}{\rho_p} \right)^{2/3} \left(\frac{a}{R_p} \right)^{7/2} \left(\frac{a}{r_c} \right)^2, \quad (\text{B.1}) \end{aligned}$$

where $F_*(t_s)$ is the inflow rate during the final satellite formation, ρ_p and ρ_s are the planet and satellite densities, R_p is the radius of the planet, and $(M_T/M_s) \sim$ a few as the satellite nears its final mass.

Next, we compute the upper limit on the characteristic impactor size, which is the size to which a particle grows due to mutual collisions with other particles before it collides with the satellite in the limit of perfect accretion. This size can be estimated by assuming that the rate of mutual collisions between the small particles is equal to the rate of collision with the satellite, or

$$\frac{\pi r_{\text{par}}^2 \sigma_{\text{par}} \Omega}{m_{\text{par}}} \sim \frac{\pi R_s^2 \sigma_s \Omega}{M_s} F_g, \quad (\text{B.2})$$

which gives $r_{\text{par}}/R_s \sim (\sigma_{\text{par}}/\sigma_s) F_g^{-1}$ for $\rho_{\text{par}} \approx \rho_s$, or

$$\begin{aligned} \frac{r_{\text{par}}}{R_s} &\sim 2 \times 10^{-6} \left(\frac{C}{10} \right)^2 \left(\frac{10^6 \text{ yr}}{\tau_{\text{in}}} \right) \left(\frac{a/R_p}{20} \right)^{7/2} \\ &\times \left(\frac{a/r_c}{0.3} \right)^2 \left(\frac{5}{F_g} \right)^2 \left(\frac{M_T}{M_s} \right), \quad (\text{B.3}) \end{aligned}$$

with $\rho_p \sim 1000 \text{ kg m}^{-3}$. Because $r_{\text{par}} \propto (1/R_s^2)$, the predicted impactor size decreases as the satellite grows. For parameter values similar to those in the Canup and Ward (2006) simulations that produce Saturn-like systems (e.g., $r_c = 30R_p$, $C \sim 15$), and with $F_g = 5$ and $\tau_{\text{in}} = 10^6 \text{ yr}$, we estimate $r_{\text{par}} \sim 10^{-6} R_{\text{Rhea}} \sim 1 \text{ m}$, comparable to the size of the largest initial inflowing particles. For the jovian satellites with $M_T \sim 2 \times 10^{-4} M_p$, $C \sim 15$, and $r_c = 30R_p$, impactor radii are $\sim 4 \text{ km}$ to 800 m for Callisto and ~ 30 to 6 m for Ganymede, decreasing by a factor of about 5 as each satellite grows from one-tenth of its final mass to its final mass. Our estimates likely give an upper limit on r_{par} because we assume that small particle collisions always result in accretion. Velocities of small particles will exceed their mutual escape velocities due to viscous stirring by the satellite, so particle–particle collisions will probably not be accretionary, which would lead to values of r_{par} smaller than our estimates here.

Implicit in our treatment of the satellite accretion rate is the assumption that the dispersion velocities of accreted particles are a constant fraction of the satellite’s time-dependent escape velocity (i.e., we consider a constant value of $F_g = 5$), and that the bulk of the satellite’s growth occurs in the “orderly” regime in which $\tau_{\text{acc}} \sim M/M \propto r$. Orderly growth implies that gravitational stirring by the large satellite dominates over stirring among the

small background particles (Goldreich et al., 2004). This would be the case throughout the majority of satellite growth in the CW model because the background particle surface density is predicted to be much smaller than the equivalent surface density of the satellite [Eq. (B.1)]. A rough estimate of the small particle dispersion velocity can be obtained by assuming that it reflects a steady-state balance between viscous stirring by the satellite and collisional damping due to particle–particle collisions, so that $(v_\infty/v_{\text{esc}}(R_s)) \sim [(\sigma_s/\sigma_{\text{par}})(r_{\text{par}}/R_s)]^{1/4}$ (Goldreich et al., 2004), which, together with Eqs. (B.1) and (B.3) gives $v_\infty \sim 0.8 v_{\text{esc}}(R_s)$. If particles do not grow beyond their initial size delivered with the inflow due to their mutual collisions, collisional damping is more effective, and $(v_\infty/v_{\text{esc}}) \sim O(0.1)$ results. In our temperature profile calculations, we set $F_g = 5$, or $v_\infty = v_{\text{esc}}/2$.

References

- Anderson, J.D., Schubert, G., 2007. Saturn’s satellite Rhea is a homogeneous mix of rock and ice. *Geophys. Res. Lett.* 34, doi:10.1029/2006GL028100. L02202.
- Anderson, J.D., Jacobson, R.A., McElrath, T.P., Moore, W.B., Schubert, G., Thomas, P.C., 2001. Shape, mean radius, gravity field, and interior structure of Callisto. *Icarus* 153, 157–161.
- Bate, M.R., Lubow, S.H., Ogilvie, G.I., Miller, K.A., 2003. Three-dimensional calculations of high- and low-mass planets embedded in protoplanetary disks. *Mon. Not. R. Astron. Soc.* 341, 213–229.
- Bizzarro, M., Baker, J.A., Haack, H., 2004. Mg isotope evidence for contemporaneous formation of chondrules and refractory inclusions. *Nature* 431, 275–278.
- Bizzarro, M., Baker, J.A., Haack, H., Lundgaard, K.L., 2005. Rapid timescales for accretion and melting of differentiated planetesimals inferred from ^{26}Al - ^{26}Mg chronometry. *Astrophys. J.* 632, L41–L44.
- Bouwman, J., Meyer, M.R., Kim, J.S., Silverstone, M.D., Carpenter, J.M., Hines, D.C., 2006. The formation and evolution of planetary systems: Placing our Solar System in context. In: Klahr, H., Brandner, W. (Eds.), *Planet Formation: Theory, Observation, and Experiments*. Cambridge University Press, New York, pp. 14–30.
- Burrows, A., Marley, M., Hubbard, W.B., Lunine, J.I., Guillot, T., Saumon, D., Freedman, R., Sudarsky, D., Sharp, C., 1997. A nongray theory of extrasolar giant planets and brown dwarfs. *Astrophys. J.* 491, 856–875.
- Canup, R.M., Ward, W.R., 2002. Formation of the Galilean satellites: Conditions of accretion. *Astron. J.* 124, 3404–3423.
- Canup, R.M., Ward, W.R., 2006. A common mass scaling for satellite systems of gaseous planets. *Nature* 441, 834–839.
- Canup, R.M., Ward, W.R., 2008. Origin of Europa and the Galilean satellites. In: *Europa after Galileo*. University of Arizona Press, Tucson, AZ, in press.
- Castillo-Rogez, J.C., Matson, D.L., Sotin, C., Johnson, T.V., Lunine, J.I., Thomas, P.C., 2007. Iapetus’ geophysics: Rotation rate, shape, and equatorial ridge. *Icarus* 190, 179–202.
- Coradini, A., Cerroni, P., Magni, G., Federico, C., 1989. Formation of the satellites of the outer Solar System: Sources of their atmospheres. In: Atreya, S.K., Pollack, J.B., Matthews, M.S. (Eds.), *Origin and Evolution of Planetary and Satellite Atmospheres*. University of Arizona Press, Tucson, AZ, pp. 723–762.
- D’Angelo, G., Henning, T., Kley, W., 2003. Thermohydrodynamics of circumstellar disks with high-mass planets. *Astrophys. J.* 599, 548–576.
- Durham, W.B., Kirby, S.H., Stern, L.A., 1997. Creep of water ices at planetary conditions: A compilation. *J. Geophys. Res.* 102, 16293–16302.
- Friedson, A.J., Stevenson, D.J., 1983. Viscosity of rock–ice mixtures and applications to the evolution of icy satellites. *Icarus* 56, 1–14.
- Garaud, P., Lin, D.N.C., 2007. The effect of internal dissipation and surface irradiation on the structure of disks and the location of the snow line around Sun-like stars. *Astrophys. J.* 654, 606–624.
- Gault, D.E., Heitowitz, E.D., 1963. The partition of energy for hypervelocity impact craters formed in rock (NASA Technical Report No. NASA-TM-X-57428). In: *Proceedings of the Sixth Hypervelocity Impact Symposium*, pp. 419–456.
- Goldreich, P., Lithwick, Y., Sari, R., 2004. Planet formation by coagulation: A focus on Uranus and Neptune. *Annu. Rev. Earth Planet. Sci.* 42, 549–601.
- Goldsby, D.L., Kohlstedt, D.L., 2001. Superplastic deformation of ice: Experimental observations. *J. Geophys. Res.* 106, 11017–11030.
- Greeley, R.C., Chyba, C., Head, J.W., McCord, T., McKinnon, W.B., Pappalardo, R.T., 2004. Geology of Europa. In: Bagenal, F., Dowling, T., McKinnon, W.B. (Eds.), *Jupiter: The Planet, Satellites and Magnetosphere*. Cambridge University Press, New York, pp. 329–362.
- Haisch Jr., K.E., Lada, E.A., Lada, C.J., 2001. Disk frequencies and lifetimes in young clusters. *Astrophys. J.* 553, L153–L156.
- Hobbs, P.V., 1974. *Ice Physics*. Clarendon Press, Oxford.
- Hubickyj, O., Bodenheimer, P., Lissauer, J.J., 2005. Accretion of the gaseous envelope of Jupiter around a 5–10 Earth-mass core. *Icarus* 179, 415–431.

- Iess, L., Rappaport, N.J., Tortora, P., Lunine, J.I., Armstrong, J.W., Asmar, S.W., Somenzi, L., Zingoni, F., 2007. Gravity field and interior of Rhea from Cassini data analysis. *Icarus* 190, 585–593.
- Kaula, W.M., 1979. Thermal evolution of growing Earth and Moon by planetesimal impacts. *J. Geophys. Res.* 84, 999–1008.
- Khurana, K.K., Russell, C.T., Dougherty, M.K., 2008. Magnetic portraits of Tethys and Rhea. *Icarus* 193, 465–474.
- Kirchoff, M.R., Schenk, P.M., 2008. Cratering records of saturnian satellites. *Lunar Planet. Sci. XXXIX*, Abstract 2234.
- Kirk, R.L., Stevenson, D.J., 1987. Thermal evolution of a differentiated Ganymede and implications for surface features. *Icarus* 69, 91–134.
- Leliwa-Kopystyński, J., Maruyama, M., Nakajima, T., 2002. The water–ammonia phase diagram up to 300 MPa: Application to icy satellites. *Icarus* 159, 518–528.
- Lewis, J.S., 1974. Interior composition and structure. In: Hunten, D. (Ed.), *The Atmosphere of Uranus*. NASA Ames Research Center, Moffett Field, CA, pp. 61–79.
- Lodders, K., 2003. Solar System abundances and condensation temperatures of the elements. *Astrophys. J.* 591, 1220–1247.
- Lubow, S.H., Seibert, M., Artymowicz, P., 1999. Disk accretion onto high-mass planets. *Astrophys. J.* 526, 1001–1012.
- Lunine, J.I., Stevenson, D.J., 1982. Formation of the Galilean satellites in a gaseous nebula. *Icarus* 52, 14–39.
- Mackenzie, R.A., Iess, L., Tortora, P., Rappaport, N.J., 2008. A non-hydrostatic Rhea. *Geophys. Res. Lett.* 35, doi:10.1029/2007GL032898. L05204.
- McEwen, A.S., Keszthelyi, L.P., Lopes, R., Schenk, P.M., Spencer, J.R., 2004. The lithosphere and surface of Io. In: Bagenal, F., Dowling, T., McKinnon, W.B. (Eds.), *Jupiter: The Planet, Satellites and Magnetosphere*. Cambridge University Press, New York, pp. 307–328.
- McKinnon, W.B., 1997. Note: Mystery of Callisto: Is it undifferentiated? *Icarus* 130, 540–543.
- McKinnon, W.B., 2006a. On convection in ice I shells of outer Solar System bodies, with specific application to Callisto. *Icarus* 183, 435–450.
- McKinnon, W.B., 2006b. Differentiation of the Galilean satellites: It's different out there. In: *Workshop on Early Planetary Differentiation*. Lunar and Planetary Institute, Houston, TX. Abstract 4053.
- McKinnon, W.B., Zolensky, M.E., 2003. Sulfate content of Europa's ocean and shell: Evolutionary considerations and some geological and astrobiological implications. *Astrobiology* 3, 879–897.
- Moore, J.M., Horner, V.M., Greeley, R., 1985. The geomorphology of Rhea: Implications for geologic history and surface processes. *J. Geophys. Res.* 90 (Supplement), C785–C795.
- Moore, J.M., Chapman, C.R., Bierhaus, E.B., Greeley, R.C., Chuang, F.C., Klemaszewski, J., Clark, R.N., Dalton, J.B., Hibbitts, C.A., Schenk, P.M., Spencer, J.R., Wagner, R., 2004. Callisto. In: Bagenal, F., Dowling, T., McKinnon, W.B. (Eds.), *Jupiter: The Planet, Satellites and Magnetosphere*. Cambridge University Press, New York, pp. 397–426.
- Mosqueira, I., Estrada, P.R., 2003. Formation of the regular satellites of giant planets in an extended gaseous nebula. I. Subnebula model and accretion of satellites. *Icarus* 163, 198–231.
- Mostefaoui, S., Lugmair, G.W., Hoppe, P., El Gorse, A., 2004. Evidence for live ^{60}Fe in meteorites. *New Astron. Rev.* 48, 155–159.
- Mueller, S., McKinnon, W.B., 1988. Three-layered models of Ganymede and Callisto—Compositions, structures, and aspects of evolution. *Icarus* 76, 437–464.
- Nagel, K., Breuer, D., Spohn, T., 2004. A model for the interior structure, evolution, and differentiation of Callisto. *Icarus* 169, 402–412.
- Nakamoto, T., Nakagawa, Y., 1994. Formation, early evolution, and gravitational stability of protoplanetary disks. *Astrophys. J.* 421, 640–650.
- Nimmo, F., Matsuyama, I., 2007. Reorientation of icy satellites by impact basins. *Geophys. Res. Lett.* 34, doi:10.1029/2007GL030798. L19203.
- O'Keefe, J.D., Ahrens, T.J., 1982. Cometary and meteorite swarm impact on planetary surfaces. *J. Geophys. Res.* 87, 6668–6680.
- Papaloizou, J.C., Nelson, R.P., 2005. Models of accreting gas giant protoplanets in protostellar disks. *Astron. Astrophys.* 433, 247–265.
- Pappalardo, R.T., Collins, G.C., Head, J.W., Helfenstein, P., McCord, T., Moore, J.M., Prockter, L.M., Schenk, P.M., Spencer, J.R., 2004. Geology of Ganymede. In: Bagenal, F., Dowling, T., McKinnon, W.B. (Eds.), *Jupiter: The Planet, Satellites and Magnetosphere*. Cambridge University Press, New York, pp. 363–396.
- Pierazzo, E., Vickery, A.M., Melosh, H.J., 1997. A reevaluation of impact melt production. *Icarus* 127, 408–423.
- Pollack, J.B., Consolmagno, G., 1984. Origin and evolution of the Saturn system. In: Bergstrahl, J.T., Miner, E.D., Matthews, M.S. (Eds.), *Saturn*. University of Arizona Press, Tucson, AZ, pp. 811–866.
- Schubert, G., Stevenson, D.J., Ellsworth, K., 1981. Internal structures of the Galilean satellites. *Icarus* 47, 46–59.
- Schubert, G., Spohn, T., Reynolds, R.T., 1986. Thermal histories, compositions, and internal structures of the moons of the Solar System. In: Burns, J.A., Matthews, M.S. (Eds.), *Satellites*. University of Arizona Press, Tucson, AZ, pp. 224–292.
- Schubert, G., Zhang, K., Kivelson, M.G., Anderson, J.D., 1996. The magnetic field and internal structure of Ganymede. *Nature* 384, 544–545.
- Schubert, G., Anderson, J.D., Spohn, T., McKinnon, W.B., 2004. Interior composition, structure and dynamics of the Galilean satellites. In: Bagenal, F., Dowling, T., McKinnon, W.B. (Eds.), *Jupiter: The Planet, Satellites and Magnetosphere*. Cambridge University Press, New York, pp. 281–306.
- Semenov, D., Helling, T., Helling, C., Ilgner, M., Sedlmayr, E., 2003. Rosseland and Planck mean opacities for protoplanetary disks. *Astron. Astrophys.* 410, 611–621.
- Showman, A.P., Malhotra, R., 1997. Tidal evolution into the Laplace resonance and the resurfacing of Ganymede. *Icarus* 127, 93–111.
- Spohn, T., Schubert, G., 2003. Oceans in the icy Galilean satellites of Jupiter? *Icarus* 161, 456–467.
- Squyres, S.W., Reynolds, R.T., Summers, A.L., Shung, F., 1988. Accretional heating of the satellites of Saturn and Uranus. *J. Geophys. Res.* 93, 8779–8794.
- Stevenson, D.J., Harris, A.W., Lunine, J.L., 1986. Origins of satellites. In: Burns, J.A., Matthews, M.S. (Eds.), *Satellites*. University of Arizona Press, Tucson, AZ, pp. 39–88.
- Tachibana, S., Huss, G.R., 2003. The initial abundance of ^{60}Fe in the Solar System. *Astrophys. J.* 588, 41–44.
- Thrane, K., Bizzarro, M., Baker, J.A., 2006. Brief formation interval for refractory inclusions and uniform distribution of ^{26}Al in the early Solar System. *Astrophys. J.* 646, L159–L162.
- Urey, H.C., 1955. The cosmic abundances of potassium, uranium, and thorium and the heat balances of the Earth, the Moon, and Mars. *Proc. Natl. Acad. Sci.* 41, 127–144.
- Wadhwa, M., Amelin, Y., Davis, A.M., Lugmair, G.W., Meyer, B., Gounelle, M., Desch, S.J., 2007. From dust to planetesimals: Implications for the solar protoplanetary disk from short-lived radionuclides. In: Reipurth, K.K.B., Jewitt, D. (Eds.), *Protostars and Protoplanets V*. University of Arizona Press and Lunar and Planetary Institute, Tucson, AZ, pp. 835–848.
- Ward, W.R., 1997. Protoplanet migration by nebula tides. *Icarus* 126, 261–281.
- Zarneck, S.E., Parmentier, E.M., 2004. The onset of convection in fluids with strongly temperature-dependent viscosity cooled from above with implications for planetary lithospheres. *Earth Planet. Sci. Lett.* 224, 371–386.
- Zimmer, C., Khurana, K.K., Kivelson, M.G., 2000. Subsurface oceans on Europa and Callisto: Constraints from Galileo magnetometer observations. *Icarus* 147, 329–347.